PNAS

Main Manuscript for

TITLE: ***Disruption of G3BP1 Granules Promotes Mammalian CNS and PNS Axon Regeneration***

AUTHORS: Pabitra K. Sahoo[1,2*], Manasi Agrawal[1,2,3], Nicholas Hanovice[4], Patricia Ward[5], Meghal Desai[2], Terika P. Smith[1], HaoMin SiMa[4], Jennifer N. Dulin[6,7], Lauren S. Vaughn[1], Mark Tuszynski[6], Kristy Welshhans[1,9], Larry Benowitz[4], Arthur English[5], John D. Houle[8], Jeffery L. Twiss[1,9*]

AFFILIATIONS:

[1] Department of Biological Sciences, University of South Carolina; Columbia, South Carolina USA.

[2] Department of Biological Sciences, Rutgers University – Newark; Newark, New Jersey USA.

[3] School of Biomedical Sciences, Kent State University; Kent, Ohio USA.

[4] Boston Children's Hospital; Cambridge, Massachusetts USA.

[5] Department of Cell Biology, School of Medicine, Emory University; Atlanta, Georgia USA.

[6] Department of Neurosciences, University of California – San Diego; LA Jolla, California USA.

[7] Department of Biology, Texas A&M University; College Station, Texas USA.

[8] Department of Neurobiology and Anatomy, Drexel University College of Medicine; Philadelphia, USA.

[9] Carolina Autism and Neurodevelopment Research Center; University of South Carolina, Columbia, South Carolina, USA.

* Corresponding Author: Pabitra K Sahoo, Ph.D.
Department of Biological Sciences
Rutgers University Newark
225 University Avenue, LSC-601C
Newark, NJ 07102 USA
phone – 1-973-353-3493
Email: pabitra.sahoo@rutgers.edu

Jeffery L Twiss, Ph.D.
Department of Biological Sciences
University of South Carolina
Columbia, SC 29208 USA

phone – 1-803-777-9215
Email: twiss@mailbox.sc.edu

Author Contributions: Conceptualization – PKS, JDH, JLT
Methodology – PKS, NH, PW, MA, MD, JDH
Investigation – PKS, NH, PW, MA, MD, JDH
Visualization – PKS, JLT
Funding acquisition – PKS, JND, MT, KW, LB, AE, JDH, JLT
Project administration – JLT
Supervision – JND, MT, KW, LB, AE, JDH, JLT
Writing, original draft – PKS, JND, JDH, PW, JLT
Writing, review & editing – NH, PW, MA, JND, MT, KW, LB, AE, JDH

Competing Interest Statement: PK Sahoo and JL Twiss hold a US patent on use of the G3BP1 cell permeable peptide for axon regeneration and neurodegeneration.

Classification: Biological Sciences/Neuroscience.

Keywords: CNS Injury, Local Protein Synthesis, G3BP1, Stress Granules, Axon Regeneration

This PDF file includes: Main Text
Main Figures 1 to 5

ABSTRACT

Depletion or inhibition of core stress granule proteins, G3BP1 in mammals and TIAR-2 in *C. elegans*, increases axon regeneration in injured neurons, showing spontaneous regeneration. Inhibition of G3BP1 by expression of its acidic or 'B-domain' accelerates axon regeneration after nerve injury, bringing a potential therapeutic intervention to promote neural repair in the peripheral nervous system. Here, we asked if G3BP1 inhibition is a viable strategy to promote regeneration in injured mammalian central nervous system where axons do not regenerate spontaneously. G3BP1 B-domain expression was found to promote axon regeneration in the transected spinal cord provided with a permissive peripheral nerve graft (PNG) as well as in crushed optic nerve. Moreover, a cell-permeable peptide (CPP) to a subregion of B-domain (rodent G3BP1 amino acids 190-208) accelerated axon regeneration after peripheral nerve injury and promoted regrowth of reticulospinal axons into the distal transected spinal cord through a bridging PNG. G3BP1 CPP promoted axon growth from rodent and human neurons cultured on permissive substrates, and this function required alternating Glu/Asp-Pro repeats

66 that impart a unique predicted tertiary structure. The G3BP1 CPP disassembles axonal G3BP1,
67 G3BP2, and FMRP, but not FXR1, granules and selectively increases axonal protein synthesis in
68 cortical neurons. These studies identify G3BP1 granules as a key regulator of axon growth in
69 CNS neurons and demonstrate that disassembly of these granules promotes retinal axon
70 regeneration in injured optic nerve and reticulospinal axon elongation into permissive
71 environments after CNS injury. This work highlights G3BP1 granule disassembly as a potential
72 therapeutic strategy for enhancing axon growth and neural repair.

73 **SIGNIFICANCE STATEMENT**

74 The central nervous system (CNS) axon does not have the capacity for spontaneous axon
75 regeneration, as seen in the peripheral nervous system (PNS). We previously showed that stress
76 granule-like aggregates of G3BP1 are present in uninjured PNS axons, and these slow nerve
77 regeneration. We now report that CNS axons contain G3BP1 granules, and G3BP1 granule
78 disassembling strategies promote axon regeneration in the injured sciatic nerve, transected
79 spinal cord with a peripheral nerve graft, and injured optic nerve. Thus, G3BP1 granules are a
80 barrier to axon regeneration and can be targeted for stimulating neural repair following
81 traumatic injury, including in the regeneration refractory CNS.

82
83 **INTRODUCTION**

84 Though the mammalian peripheral nervous system (PNS) can spontaneously regenerate
85 injured axons, the growth rates are extremely slow at about 1-4 mm/day (1). Regenerating PNS
86 axons can successfully navigate to their targets over short distances and restore at least partial
87 function. However, PNS nerve regeneration for distances more than 5-6 cm is much less
88 successful; this has been attributed to a progressive decline of the growth-supportive
89 environment of the distal nerve and/or the receptivity of target tissues for reinnervation (1).
90 Successful axon regeneration in the central nervous system (CNS) is even more problematic, as

91 CNS neurons have a considerably lower intrinsic growth capacity than PNS neurons and the
92 extracellular environment of the injured CNS actively inhibits axon regeneration (2). Thus, there
93 are unmet clinical needs to accelerate PNS axon regeneration and to enable
94 CNS axon regeneration.

95 Activation of the mTOR pathway, which increases overall cap-dependent protein
96 synthesis, has been shown to promote axon regeneration in the injured CNS and PNS (3-9).
97 Indeed, deletion or inhibition of PTEN that increases activity of the mTOR pathway promotes
98 regeneration of corticospinal tract axons in the injured spinal cord that are typically among the
99 most refractory to regeneration (7). Protein synthesis in axons has been shown to facilitate PNS
100 axon regeneration (10). Intra-axonal protein synthesis is a well-established mechanism in
101 cultured CNS neurons, where the axon uses locally synthesized proteins for directional growth;
102 there are now multiple lines of evidence indicating that many CNS neurons retain the capacity
103 for intra-axonal protein synthesis well into adulthood (11-13), and some evidence for mRNA
104 translation in spinal cord axons (14-17). We previously showed that axonal RNA-protein
105 granules containing the core stress granule protein G3BP1 slow PNS axon regeneration by
106 sequestering mRNAs and attenuating their translation in injured axons (18). Stress granules,
107 which form by liquid-liquid phase separation (LLPS), are typically seen during metabolic or
108 oxidative stress conditions and are used to store mRNAs encoding proteins that are not needed
109 to respond to the stress (19). However, axons use stress granule-like structures as RNA storage
110 depots in the apparent absence of any stress signals (18, 20), and disassembly of axonal G3BP1
111 granules promotes intra-axonal protein synthesis and accelerates PNS axon regeneration (18,
112 20). Here, we asked whether inhibiting the RNA sequestration function of G3BP1 has
113 therapeutic potential for promoting CNS axon regeneration.

114 **RESULTS**

115 ***G3BP1 granules attenuate axon regeneration in the central nervous system***.

116 We previously showed that G3BP1 granules slow PNS axon regeneration and that
117 expressing G3BP1's acidic domain or 'B-domain', consisting of rat G3BP1 amino acids 141-220
118 (UniProt ID: D3ZYS7_RAT), accelerates axon regeneration following sciatic nerve crush injury
119 (18). G3BP1 B-domain expression decreases both the size and number of axonal G3BP1
120 granules, increases intra-axonal protein synthesis in cultured sensory neurons, and accelerates
121 PNS nerve regeneration (18). Thus, the exogenously expressed G3BP1 B-domain acts as a
122 'dominant negative' agent. With these effects seen in PNS axons when G3BP1 is inhibited, we
123 hypothesized that axonal G3BP1 granules could also impede CNS axon regeneration.

124 Neural stem cells have been shown to promote CNS axon growth, where injured
125 corticospinal axons can regrow to form a relay circuit across a site of spinal cord injury by
126 forming synapses on stem cell-derived neurons grafted into the lesion site (21, 22). Lu *et al.*
127 (2012) showed that neural progenitor cells isolated from the embryonic spinal cord ('caudalized
128 grafts') promote growth of host corticospinal motor axons, whereas neural progenitor cells
129 isolated from the embryonic telencephalon ('rostralized grafts') do not support regeneration
130 into the graft (21). Using immunofluorescence for G3BP1 and TIA1, another core stress granule
131 protein, we find that corticospinal axons in injured spinal cord contain more G3BP1-TIA1
132 granules in animals with a rostralized progenitor graft, which does not support regeneration,
133 than those with a caudalized progenitor graft (**Fig. 1A**). This emphasizes that spinal cord axons
134 contain G3BP1 and TIA1 granules, and that the abundance of these intra-axonal stress granule-
135 like structures relatively decreases when a regeneration-promoting stimulus is provided to the
136 injured spinal cord axons.

137 Adult dorsal root ganglion (DRG) sensory neurons and embryonic cortical neurons from
138 rats show increased axon growth upon disassembly of G3BP1 granules induced by expression of
139 the G3BP1 B-domain in culture (18). To test the possibility that G3BP1 granules may negatively
140 influence the growth of adult CNS axons, we asked whether B domain expression would
141 increase rates of injured spinal cord axon growth within a permissive growth environment. For
142 this, we transduced reticulospinal neurons using adeno-associated virus (AAV), serotype 5
143 expressing G3BP1 B-domain-blue fluorescent protein (BFP), full length G3BP1-BFP, or GFP.
144 Fifteen days later, a C4 hemisection was performed and a peripheral nerve graft (PNG) was
145 apposed to the rostral injury site adjacent to the reticulospinal tract as a growth-permissive
146 environment (**Fig. 1B**). Immunofluorescence for axons performed at 20 days after spinal cord
147 injury/PNG placement showed more axons extending further distances from the spinal
148 cord/PNG apposition in the G3BP1 B-domain-BFP expressing animals compared to the G3BP1-
149 BFP and GFP expressing animals (**Fig. 1C-D**). These data indicate that G3BP1 B-domain
150 expression can promote adult CNS axon growth *in vivo*.
151 The axons regenerating in the PNG above provide some similarities for spinal motor
152 axons regenerating in peripheral nerve – *i.e.*, the descending reticulospinal neurons regenerated
153 their axons through a growth-permissive PNS environment. Thus, we moved to an optic nerve
154 injury model where CNS neurons must regenerate their axons through a growth-inhibitory CNS
155 environment. For this, retinal ganglion cells (RGC) were transduced via intravitreal injection
156 with AAV serotype 2 (AAV2) expressing G3BP1 B-domain-BFP, G3BP1-BFP, or GFP, and then
157 crushed the optic nerve 14 days later (**Fig. 1E**). 14 days after this injury, immunofluorescent
158 staining for growth-associated protein 43 (GAP43) to detect regenerating axons and BFP/GFP to
159 detect transduced neurons showed that G3BP1 B-domain expression in RGCs greatly increases

160 axon regeneration (**Fig. 1F-G**). Interestingly, animals expressing the G3BP1 B-domain appeared
161 to show far higher number of axons proximal to the injury site (**Fig. 1F**). Evaluation of
162 transduction efficiency based on optic nerve BFP positivity showed equivalent axon percentages
163 for G3BP1-BFP vs. G3BP1 B-domain-BFP (**Suppl. Fig. S1A-B**).

164 Expression of G3BP1 B-domain in PNS neurons disassembles axonal G3BP1 granules and
165 in turn accelerates PNS nerve regeneration (18). To determine if expression of the G3BP1 B-
166 domain affects G3BP1 granules in CNS axons, we compared G3BP1 granules in the reticulospinal
167 axons in PNGs and RGC axons in the injured optic nerve using confocal microscopy where we
168 could extract G3BP1 granule signals that overlapped with axonal markers across optical planes
169 as a separate panel (projected XYZ images shown for 'Axonal G3BP1' panels in **Suppl. Fig. S1C**
170 **and F**). G3BP1 B-domain expression in reticulospinal neurons and RGCs resulted in smaller and
171 fewer G3BP1 granules in the axons compared to G3BP1 and control GFP expression (**Suppl. Fig.**
172 **S1D-E and G-H**). In contrast to many other CNS and PNS axotomies, optic nerve crush triggers
173 death in the majority of RGCs (23-26), and we find that transduction with AAV2-G3BP1 B-
174 domain-BFP increased post-injury RGC survival compared to the two control conditions (**Suppl.**
175 **Fig. S2**). Taken together, these findings indicate that expression of the G3BP1 B-domain can
176 facilitate regeneration of injured CNS axons and overcome the growth-inhibitory environment of
177 the injured CNS, likely through G3BP1 granule disassembly and release of axonal mRNAs for
178 translation.

179 ***Cell permeable G3BP1 B-domain peptide increases PNS nerve regeneration.***

180 Using synthetic cell-permeable peptides (CPP), we previously found that amino acids
181 147-166 and 190-208 of rat G3BP1 increase axon growth from cultured sensory and cortical
182 neurons (18), whereas a CPP consisting of rat G3BP1 amino acids 168-189 had no significant

183 effect (18). G3BP1 amino acid sequences for 147-166 and 190-208 CPPs are quite acidic with
184 Glu or Asp residues occupying 11 of 21 (52.4%) and 8 of 19 residues (42.1%), respectively (**Fig.**
185 **2A**). The G3BP1 190-208 CPP was more effective than 147-166 CPP in our earlier study (18), so
186 we tested whether the G3BP1 190-208 CPP might affect PNS axon regeneration *in vivo* using a
187 clinically relevant paradigm where the CPP is applied after nerve injury. For this, a mid-thigh
188 sciatic nerve crush was performed on adult rats and 2 days later the G3BP1 190-208 or 168-189
189 CPP was injected just proximal to the injury site to achieve an estimated 113 μM concentration
190 within the perineurium (**Fig. 2B**). G3BP1 190-208 CPP-injected animals showed a strong increase
191 in axon regeneration at 7 days post-injury (5 days after peptide treatment) compared to G3BP1
192 168-189 CPP-injected animals, an effect that was particularly evident at longer distances down
193 the nerve (**Fig. 2C-D**). The G3BP1 168-189 CPP-injected animals showed no significant difference
194 from those injected with an equivalent volume of the vehicle control (phosphate-buffered saline
195 [PBS]; **Fig. 2D**).
196 To determine if the accelerated nerve regeneration seen with the G3BP1 190-208 CPP
197 brings functional improvements, we compared neuromuscular junction reinnervation in G3BP1
198 168-189 vs. 190-208 CPP-treated animals using compound muscle action potentials (CMAP) for
199 the lateral gastrocnemius (LG) and tibialis anterior (TA) muscles (**Fig. 2B**). Recovery of CMAPs
200 was significantly accelerated in the animals treated with G3BP1 190-208 CPP treatment for both
201 the LG and TA at 2 and 4 weeks after sciatic nerve crush (**Fig. 2E, Suppl. Fig. S3A**). There were
202 no differences between the G3BP1 190-208 and 168-189 CPP-treated animals at 8 weeks post-
203 injury (**Fig. 2E**), consistent with spontaneous regeneration in the PNS; similar results were
204 previously reported for sciatic nerve crush recovery in AAV-G3BP1 B-domain transduced animals
205 (18). It should be noted that significant differences between the G3BP1 190-208 and 168-189

206 CPP-treated animals were not seen at 6 weeks post-injury, which points to a limited *in vivo*
207 duration for the G3BP1 190-208 CPP activity and emphasizes an opportunity to improve peptide
208 stability.

209 The G3BP1 190-208 sequence contains seven Glu-Pro (EP_7) repeats flanked by N-
210 terminal Val-Val and C-terminal Val-Ser-Asp (**Fig. 2A**). We sought to determine critical residues
211 for function of the 190-208 G3BP1 CPP by asking whether sequence alterations modified its
212 axon growth-promoting activity in adult DRGs cultured on laminin. We initially tested 190-208
213 G3BP1 CPP from a different vendor ('Bachem') and got identical results to the previous synthetic
214 peptide (**Fig. 2F, Suppl. Fig 3B-D**). A modified 190-208 CPP in which all Glu residues in the EP_7
215 region were replaced with similarly acidic Asp residues promoted axon growth to a similar
216 extent as the original 190-208 CPP (**Fig. 2F, Suppl. Fig. S3B-D**). Similarly, a CPP lacking the N-
217 and C-terminal residues flanking the EP_7 repeats (G3BP1 192-205 CPP) maintained full axon
218 growth-promoting activity (**Fig. 2F, Suppl. Fig. S3B-D**), indicating that just the seven EP repeats
219 are sufficient to promote axon growth. However, a scrambled 190-208 G3BP1 CPP where the
220 EP_7 was changed to seven Glu followed by seven Pro (E_7P_7) generated axon lengths that were
221 not significantly different than the non-functional 168-189 G3BP1 CPP (**Fig. 2F, Suppl. Fig. S3B-**
222 **D**). Taken together, these data indicate that axon growth-promoting functions of the 190-208
223 G3BP1 CPP require repeats of acidic residues with intervening Pro.

224 The G3BP1 147-166 sequence bears some similarities to the 190-208 sequence with a
225 preponderance of Glu residues (**Fig. 2A**). Interestingly, we have shown that Casein kinase 2
226 alpha (CK2α)-dependent phosphorylation of G3BP1 on Ser 149 ($G3BP1^{PS149}$) causes G3BP1
227 granule disassembly and decreases G3BP1's RNA binding activity (20). Considering the
228 functional effects of Ser 149 phosphorylation, we asked whether replacing Ser 149 with an

229 acidic residue to mimic phosphorylated G3BP1 (147-177^{S149E}) would increase the axon growth
230 effects of G3BP1 147-166 CPP to levels comparable to the G3BP1 190-208 CPP. G3BP1 147-
231 149^{S149E} CPP treatment generated axon lengths intermediate between the 168-189 and 190-208
232 CPPs (**Fig. 2F, Suppl. Fig. S3B-D**), indicating that the S149E modification did not raise the 147-
233 166 CPP's efficacy to that of the 190-208 CPP. We further tested a CPP containing the human
234 G3BP1 sequence corresponding to rat amino acids 190-208 (human 191-209). The human 191-
235 209 CPP promoted axon growth comparable to the rat 190-208 CPP despite an Asp at residue
236 197 (instead of Glu) and Gln at residue 204 (instead of Pro) within the EP_7 region (**Fig. 2A and F,**
237 **Suppl. Fig. S3B-D**). Rat 190-208, rat 192-205 (EP_7), and human 191-209 CPPs also substantially
238 increased neurite growth from glutamatergic neurons derived from human induced pluripotent
239 stem cells (hiPSC) (**Fig. 2G, Suppl. Fig. S4**).
240 Axon branching in adult DRG cultures treated with the G3BP1 CPP variants was also
241 assessed. The rat 192-205, human 191-209, and rat 147-166^{S149E} G3BP1 CPPs increased branch
242 density by ~12% as compared to the rat 190-208 and other CPP variants, which were not
243 different than the rat 168-189 CPP with no axon outgrowth effects (**Suppl. Fig. S3D**). Similarly,
244 rat 192-205 and human 191-209 G3BP1 CPPs increased neurite branch density in the hiPSC-
245 derived neurons, but the rat 190-208 and scrambled 190-208 G3BP1 CPPs were no different
246 than the rat 168-189 CPP or no treatment control (**Suppl. Fig. S4C**). Notably, each of the CPPs
247 that increased the total axon/neurite length also increased the length of the longest
248 axon/neurite per neuron (**Suppl. Figs. S3C and S4B)**, indicating that the increased branching
249 seen with rat 192-205 and human 191-209 CPPs does not account for the difference in total
250 axon/neurite lengths shown above. In contrast, the increase in DRG total axon length and
251 longest axon per neuron induced by the rat 147-166^{S149E} CPP was modest with non-significant Z

252 score compared to the population mean, suggesting that it had minimal effects on elongating

253 axon growth (**Fig. 2F, Suppl. Fig. S3C-D**).

254 ***G3BP1 190-208 cell-permeable peptide differentially alters CNS axon regeneration depending***
255 ***on the local environment.***

256 Since the G3BP1 190-208 CPP successfully promotes PNS axon regeneration (**Fig. 2B-E**)
257 and the G3BP1 B-domain promotes regeneration of reticulospinal axons (**Fig. 1B-D**), we asked
258 whether this CPP strategy might also be effective in promoting CNS axon regeneration. To test
259 this, we performed a C4 hemisection with a PNG apposed close to the rostral injury site for axon
260 growth by descending axons or local interneurons (**Fig. 3A**). The same day, the rat 168-189 or
261 190-208 G3BP1 CPPs were injected directly into the spinal cord just rostral to the injury site and
262 regeneration through the PNG was evaluated 10 days later by immunostaining for axonal
263 markers (**Fig. 3A**). Increases in axon profile numbers were only seen in the most proximal
264 segment of the PNG for the G3BP1 190-208 compared to 168-189 CPP-treated animals (**Fig. 3B**).
265 Thus, in contrast to the effect of the G3BP1 B-domain in this experimental model, there were no
266 differences between treatment groups in the more distal PNG segments (2-6 mm; **Fig. 3B**).
267 Confocal microscopy for XYZ imaging of the proximal PNG segment was used to reconstruct the
268 path and branches of individual regenerating axons across optical planes representing cross
269 sections of the PNG in combination with *NeuroLucida* software neurite tracking/branching
270 function. Surprisingly, the 190-208 G3BP1 CPP-treated animals showed a remarkable increase in
271 axon branching complexity in the proximal PNG compared to the 168-189 CPP-treated animals
272 (**Fig. 3C-D**). Thus, although the 190-208 G3BP1 CPP increases axon outgrowth in PNGs, this
273 appears to result in axon branching or sprouting rather than the axon elongation seen in PNGs
274 with AAV-G3BP1 B-domain transduced reticulospinal neurons.

275 In the above spinal cord injury experiment, the CPPs were presented to axons directly in
276 the injured spinal cord but the nerve regeneration experiments in Figure 2 presented the CPPs

277 to axons in the permissive environment of the peripheral nerve. Thus, we asked if exposing
278 regenerating reticulospinal axons to G3BP1 CPPs within the PNG might alter their growth
279 differently. For this, we performed a C4 hemisection with descending PNG as in Figure 1; 30
280 days later, CPPs were injected into the distal PNG that was then apposed to the spinal cord
281 adjacent to the caudal injury site (**Fig. 3E**). Animals were euthanized 22 days later (52 days post-
282 injury, 22 days CPP exposure) and spinal cords with attached PNG were analyzed for axon
283 regeneration using SCG10 immunostaining. The 190-208 G3PB1 CPP-treated animals showed
284 increased numbers of axons entering into the spinal cord from the PNG, and those axons
285 extended considerably greater distances into the spinal cord compared to scrambled 190-208
286 CPP-treated animals (**Fig. 3F-G**). Thus, the 190-208 G3BP1 CPP can promote growth of injured
287 adult spinal cord axons, but our data suggest that it generates different growth morphologies
288 depending on whether the CPP is presented in the growth-inhibitory environment of the spinal
289 cord or the growth-permissive environment of the PNG.

290 ***Axonal growth morphology induced by G3BP1 190-208 cell permeable peptide depends on***
291 ***growth environments.***

292 To directly test the possibility that the G3BP1 190-208 CPP differentially alters axon
293 growth depending on the permissiveness of the growth substrate, we evaluated neurite growth
294 from embryonic day 18 (E18) rat cortical neurons cultured on growth-permissive (poly-D-lysine
295 [PDL]) or growth-inhibitory (PDL + aggrecan) substrates. For neurons cultured on PDL, rat 190-
296 208 G3BP1 CPP nearly doubled total axon length and distance the axon extended from the
297 soma, had a smaller but significant effect on dendrite lengths, and decreased axon and dendrite
298 branching compared to 168-189 CPP (**Fig. 4A, Suppl. Fig. S5**). In contrast, 190-208 G3BP1 CPP-
299 treated cortical neurons cultured on PDL + aggrecan showed increased axon and dendrite

300 branching compared to 168-198 CPP-treated neurons (**Fig. 4B**). Total axon and dendrite lengths
301 were increased by 25% and 80%, respectively, for the 190-208 G3BP1 CPP-treated compared to
302 168-198 CPP-treated cortical neurons cultured on PDL + aggrecan; distance extended from the
303 soma was not changed for the axons but was increased for the dendrites in these CNS neurons
304 (**Fig. 4B, Suppl. Fig. S5B**). We had previously shown that G3BP1 190-208 CPP treatment
305 increases axon lengths for DRG neurons grown on laminin (18). In contrast to the cortical
306 neurons used above, DRG neurons only extend $Tau^{+}/MAP2^{-}$ neurites with other axonal features
307 (27-29) in culture, so only axon growth can be evaluated in these DRG cultures. 190-208 G3BP1
308 CPP-treated DRG cultures showed increased total axon length on laminin + aggrecan, but axon
309 branching was also significantly increased compared to the 168-189 CPP-treated neurons
310 (**Suppl. Fig. S5C-D**). Taken together, these data indicate that disassembling axonal G3BP1
311 granules using the 190-208 G3BP1 CPP in non-permissive growth environments increases
312 neurite branching, while the CPP promotes elongating axon growth in permissive growth
313 environments.

314 Axon growth-inhibiting vs. -promoting substrates are known to differentially regulate
315 activities of the small GTPases RhoA, Rac, and CDC42 (30-34). CSPGs, in particular, activate
316 RhoA in distal axons, which promotes actin filament disassembly and growth cone retraction (2),
317 and accordingly, inhibition of RhoA allows axons to grow on this non-permissive substrate (35-
318 37). In contrast, axon growth-promoting stimuli (*e.g.*, neurotrophins) activate Rac and CDC42 in
319 distal axons, which promotes actin filament assembly and growth cone advance (34). To
320 determine if RhoA plays any role in the increased axon branching seen with rat 190-208 G3BP1
321 CPP treatment for neurons grown on the CSPG aggrecan, we pharmacologically inhibited RhoA
322 kinase (ROCK) using the ROCK inhibitor Y27632 (10 µM) in E18 rat cortical neurons cultured on

323 PDL + aggrecan simultaneously with CPP treatment. As Y27632 has been previously shown to
324 increase neurite growth of both PNS and CNS neurons on growth non-permissive substrates (38-
325 40), we focused on a combinatorial treatment of the neurons with Y27632 and CPP. For the
326 control CPP-treated neurons (scrambled 190-208 G3BP1), RhoA inhibition increased total axon
327 length/neuron, but this can be attributed to an approximately five-fold increase in axon
328 branching compared to vehicle-treated neurons (DMSO; **Fig. 4C-D, Suppl. Fig. S5E**). For the rat
329 190-208 G3BP1 CPP-treated neurons, RhoA inhibition increased total axon length, but decreased
330 axon branching compared to DMSO-treated cultures (**Fig. 4D, Suppl. Fig. S5E**). Together, these
331 data indicate that RhoA activity drives axon branching on the growth-inhibitory substrate in the
332 presence of the G3BP1 granule disassembling CPP. This raises the interesting possibility that
333 intra-axonal signaling, driven by the permissiveness vs. non-permissiveness of the axon's
334 environment, can shift the elongating morphology of CNS axon growth depending upon RhoA
335 activity and G3BP1 granule formation status.

336 ***G3BP1 192-205 cell permeable peptide disassembles specific axonal RNPs and enhances***
337 ***axonal protein synthesis.***

338 Previously, we have shown that the expression of the G3BP1 B-domain in NIH-3T3 cells
339 blocks arsenite-induced SG formation (18). Moreover, the application of the G3BP1 190-208
340 CPP to DRG neurons leads to immediate disassembly of axonal G3BP1 granules and specifically
341 increases axonal protein synthesis (18). In Figure 2, we identified that the core 192-205 (EP_7)
342 peptide of rat G3BP1 is equally effective as the 190-208 peptide. Based on these data, we asked
343 if the G3BP1 granule disassembling 192-205 (EP_7) CPP works in a similar manner in CNS neurons.
344 For this, we treated 10 days in vitro (DIV) embryonic rat cortical neuron cultures with scrambled
345 (E_7P_7) or G3BP1 192-205 (EP_7) CPP for 1 h and then assayed the effect of the CPPs on G3BP1 and

346 other stress granule proteins by confocal microscopy. The G3BP1 192-205 (EP_7) CPP significantly
347 reduces both the density and size of axonal G3BP1 granules (**Fig. 5A-C**). G3BP2 and FMRP axonal
348 granule density were decreased by the 192-205 (EP_7) CPP, but granule size was not affected (**Fig.**
349 **5D-F**, **Suppl. Fig. S6A-C**). Interestingly, the G3BP1 192-205 (EP_7) CPP did not show any significant
350 effect on axonal FXR1 granule density or size (**Suppl. Fig. S6D-F**). Overall, these data indicate
351 that the G3BP1 CPP promotes the disassembly of axonal LLPS for multiple stress granule-linked
352 proteins.

353 We previously showed that the 190-208 G3BP1 CPP increases axonal but not cell body
354 protein synthesis in adult DRG neurons (18). Thus, we asked if the G3BP1 192-205 (EP_7) CPP can
355 modulate protein synthesis in CNS neurons. 30 min exposure to the G3BP1 192-205 (EP_7) CPP
356 specifically increases axonal protein synthesis in 10 DIV embryonic rat cortical neuron cultures
357 without any significant effect on soma protein synthesis (**Fig. 5G-I**). Because this peptide also
358 penetrates glial cells, we asked if protein synthesis in Schwann cells of mixed adult DRG cultures
359 would be affected by G3BP1 192-205 (EP_7) CPP treatment. There was no significant change in
360 protein synthesis in the Schwann cells by puromycinylation comparing 192-205 (EP_7) vs.
361 scrambled (E_7P_7) CPP-treated cultures (**Suppl. Fig. S6G-H**). Taken together, these data suggest
362 that the G3BP1 granule disassembling CPP specifically increases protein synthesis in the axonal
363 compartment.

364 Considering the effect of RhoA inhibition shown in Figures 4 and S5, we asked if the
365 G3BP1 granules in cortical neurons contain *RhoA* mRNA and if this interaction is affected by
366 growth-inhibiting vs. growth-promoting stimuli. Analysis of RNA coimmunoprecipitating with
367 G3BP1 (i.e., RNA co-immunoprecipitation or RIP) by reverse-transcriptase droplet-digital PCR
368 (RT-ddPCR) data shows that treatment of cortical neurons with aggrecan significantly reduces
369 the interaction of *Rhoa* mRNA with G3BP1 and the G3BP1 192-205 (EP_7) CPP has no apparent

370 effect on G3BP1-*Rhoa* interaction (**Fig. 5K**, **Suppl. Fig. S6I**). Considering the known role of the
371 mTor pathway in modulating CNS and PNS axon growth (3-9), we asked if *mTor* and *Pten* mRNAs
372 might show G3BP1 association that is altered by growth-inhibiting vs. growth-promoting stimuli.
373 Treatment with laminin, aggrecan, or the G3BP1 192-205 (EP_7) CPP attenuated G3BP1-*mTor*
374 mRNA interaction but had no significant effect on G3BP1-*Pten* mRNA interaction (**Fig. 5L, M**).
375 Taken together, these data emphasize that the specificity of response to G3BP1 granule
376 disassembly is modulated by the neuronal growth environment, providing a likely explanation
377 for the differences in axon growth promotion seen with granule disassembly in CNS vs. PNS
378 extracellular environments.

379 **DISCUSSION**

380 In contrast to the PNS, low capacity for axon growth after injury combined with a
381 growth-inhibitory extracellular milieu in the injured brain and spinal cord limits the mature CNS
382 neurons' axon regeneration after traumatic CNS injuries (2). Consequently, interventions are
383 needed to coax CNS axons to regenerate. PNS axons can spontaneously regenerate but grow
384 very slowly at 1-4 mm per day (1). We previously showed that decreasing LLPS of RNA-protein
385 granules containing the core stress granule protein G3BP1 accelerates the regeneration of
386 injured PNS axons (18, 20). Here, we show that expression of G3BP1's conserved B-domain
387 (amino acids 141-220) accelerates regeneration of reticulospinal axons in the growth-permissive
388 environment of a peripheral nerve grafted into the hemisected spinal cord and is sufficient to
389 enable injured RGCs to regenerate axons in the growth-inhibitory CNS environment of the
390 injured optic nerve. We previously found that this B-domain functions as a dominant negative
391 agent by preventing axonal G3BP1 granule assembly and increasing axonal protein synthesis
392 (18). Since G3BP1 B-domain expression in reticulospinal neurons and RGCs decreased granule

393 formation by endogenous G3BP1 in their axons, G3BP1 B-domain expression in the CNS neurons
394 likely increases regeneration by releasing axonal mRNAs encoding regeneration-associated
395 proteins that are normally sequestered in G3BP1 granules. Notably, depletion of the *C. elegans*
396 orthologue of TIA1, TIAR-2, similarly increased regeneration following axotomy by decreasing
397 RNA-protein granules and increasing axonal protein synthesis (41). Together with the findings
398 herein, this observation emphasizes that mRNA sequestration impedes mammalian CNS axon
399 regeneration just as previously shown for mammalian PNS nerve and for invertebrate axon
400 regeneration (18, 41).

401 Some interventions that increase PNS axon regeneration have proven successful for
402 promoting CNS axon regrowth, though this is often limited in terms of the extent of growth
403 promotion. For example, conditioning lumbosacral sensory neurons by sciatic nerve crush injury
404 accelerates axon regeneration after subsequent PNS injury and brings a degree of axon
405 regrowth after dorsal column lesion in the spinal cord (42). This phenomenon is attributable to
406 the entry of inflammatory cells into the injured PNS, which elevates levels of cell-derived growth
407 factors including oncomodulin and SDF-1 (43). The PTEN→mTOR pathway has been
408 manipulated to increase CNS and PNS axon regeneration either by attenuating PTEN activity or
409 downstream interventions that more directly increase mTOR activity (4, 7). PTEN activity can
410 modify gene transcription (44), however, the increase in mTOR activation with PTEN deletion
411 also converges on the translation machinery to globally increase cap-dependent protein
412 synthesis (45). The resulting activation of the mTOR pathway can promote axon regeneration
413 even in injured corticospinal tract axons that normally show very poor growth (8). *mTor* mRNA
414 is locally translated in PNS axons in response to an injury-induced increase in axoplasmic Ca^{2+}
415 (20, 46). This increase in axonal mTOR protein supports neuronal survival after injury (46) but is

416 also needed for subsequent translation of axonal *Csnk2a1* mRNA, with newly generated CK2α
417 phosphorylating G3BP1 and triggering G3BP1 granule disassembly to increase axonal protein
418 synthesis (20). *mTor* mRNA is also locally translated in axons of cultured cortical neurons (47)
419 and the mRNA and protein are present in growth cones of developing CNS neurons *in vivo* (48).
420 We find that *mTor* mRNA coprecipitates with neuronal G3BP1 protein and exposure to either
421 aggrecan or laminin depletes the mRNA from G3BP1 interaction. *mTor* mRNA was also released
422 from G3BP1 interaction by the G3BP1 granule disassembling CPP. In contrast to PNS and other
423 CNS neurons, a large proportion of RGCs die after optic nerve injury; similar to what we show
424 with G3BP1 B-domain expression in RGCs, deletion of the murine *PTEN* gene was shown to
425 increase survival of axotomized RGCs in addition to promoting regeneration (9). Thus, aggrecan-
426 induced release of *mTor* mRNA from G3BP1 interaction upon G3BP1 granule disassembly may
427 indeed prevent the death of injured RGCs that were transduced with the AAV2-G3BP1 B-
428 domain.

429 Though we have previously shown that G3BP1 B-domain and 190-208 CPP decrease
430 axonal G3BP1 granules and increase translation of protein products that promote axon growth
431 (18), it is not yet clear how either disrupts the G3BP1 granules. The B-domain is one of G3BP1's
432 three intrinsically disordered regions (IDR) and is required for LLPS by G3BP1 (49). This region is
433 well-conserved across vertebrate species, with mouse showing more than 85% homology to
434 human, 67% to xenopus, and 46% to zebrafish based on G3BP1 sequences available in UniProt
435 (50). The rodent 190-208 and human 191-209 sequences lie within G3BP1's IDR1, which
436 intramolecularly interacts with the protein's IDR3 (49, 51). CPPs have been employed to disrupt
437 protein-protein interactions (52). For example, CPPs were used to disrupt mutant Huntingtin's
438 (HTT) protein-protein interactions in a Huntington disease model and DJ-1's (PARK7)

439 interactions in a Parkinson disease model (53, 54). Though the G3BP1 B-domain (IDR1) was
440 shown to intramolecularly interact with the protein's IDR3 (49, 51), we do not detect
441 coprecipitation of G3BP1 with a biotinylated 190-208 G3BP1 CPP, even when testing
442 recombinant G3BP1 combined with crosslinking (raw data will be submitted to https://odc-
443 sci.org). Thus, interruption of G3BP1's intramolecular interactions or interactions of multiple
444 G3BP1 proteins with one another is an unlikely mechanism. G3BP1 is a core stress granule
445 protein that we previously showed interacts with other stress granule proteins in PNS sensory
446 axons including TIA1 (18). We show that core functional amino acids of the G3BP1 CPP (i.e., the
447 EP_7 repeat region, rat amino acids 192-205) disrupts G3BP1, G3BP2, and FMRP, but not FXR1
448 granules, in axons of cultured cortical neurons. Similar to the CPP not binding to G3BP1, we also
449 do not see coprecipitation of G3BP2 with the 190-208 CPP (raw data will be submitted to
450 https://odc-sci.org); thus, future studies will be needed to determine how the 190-208 CPP
451 disassembles G3BP1 granules. Depletion and knockout approaches have defined several core
452 stress granule proteins and proximity biotinylation approaches have uncovered many G3BP1
453 interacting proteins (49, 51, 55-57). Axonal G3BP1 colocalizes with TDP43, and rodent 190-208
454 G3BP1 CPP triggers disassembly of pathological TDP43 aggregates in axons of iPSC-derived
455 human motor neurons (58). Additionally, G3BP1 binds to the adapter protein Annexin A11,
456 which allows the RNP complex to be transported along axons by hitchhiking on
457 lysosomes/endosomes as a means for delivering mRNAs into axons (59). Since we see that
458 sustained exposure to the 190-208 G3BP1 CPP facilitates axon growth and delivery of new
459 mRNAs into axons that are needed for regeneration (10), the 190-208 CPP likely does not
460 interrupt G3BP1-AnnexinA11 interactions. Additional studies beyond the structure-activity

461 relationship analyses included here will be needed to uncover how the G3BP1 CPP and B-
462 domain disrupt G3BP1 granules.

463 The rodent 190-208 G3BP1 CPP contains seven Glu-Pro repeats, and a CPP with just the
464 seven Glu-Pro repeats (rodent G3BP1 amino acids 192-205) is sufficient for neurite growth-
465 promoting activity. Acidic residues with alternating prolines are essential for this growth
466 promotion, because a CPP with Asp residues replacing Glu has full activity, but its activity is lost
467 on scrambling the Glu-Pro repeats. Tertiary structures of rodent 190-208 and human 191-209
468 G3BP1 sequences generated with *Pepfold3* (60-62) predict a kink in the peptide backbone at
469 each Pro with the acidic side chains of each acidic residue projecting peripherally from the
470 backbone (**Suppl. Fig. S3Ei-ii**), which is lost in the scrambled rodent 190-208 G3BP1 CPP (**Suppl**
471 **Fig. S3Eiii**). These predicted 3D structure differences of the rodent 190-208 and human 191-209
472 G3BP1 CPPs compared to scrambled rodent 190-208 CPP, as well as the rodent 147-168^{S149E}
473 G3BP1 CPP (**Suppl. Fig. S3Eiv**), may contribute to differences in their growth promoting abilities.

474 It is intriguing that the 190-208 peptide increased branching of axons in the PNGs when
475 presented in the non-permissive environment of the injured spinal cord (**Fig. 3A-D**) and for
476 primary neurons cultured on non-permissive CSPG substrate compared to elongating growth on
477 permissive laminin substrate (**Fig. 4B, Suppl. Fig S5A-D**). This effect is in contrast to G3BP1 B-
478 domain expression that must begin before injury – this may point to different mechanisms
479 underlying prevention of G3BP1 granule formation (i.e., viral-based B-domain expression before
480 injury) vs. disassembly of formed G3BP1 granules (i.e., 190-208 G3BP1 CPP administration after
481 injury). Interestingly, inhibition of ROCK partially reversed the increased branching seen in the
482 190-208 G3BP1 CPP-treated neurons grown on aggrecan (**Fig. 4C-D, Suppl. Fig S5E**). Activation
483 of RhoA causes actin filament disassembly (63), and *RhoA* mRNA is locally translated in axons

484 (64) with previous studies showing that CSPGs stimulate axonal *RhoA* mRNA translation in axons
485 (31). This raises the possibility that the axon's environment determines either the complement
486 of mRNAs released from G3BP1 granules or which released mRNAs are translated in the axons.
487 *RhoA* mRNA has been detected in G3BP1-RNA coimmunoprecipitations (65). Axon branching
488 requires local reorganization of the cytoskeleton (66), and increasing RhoA protein locally could
489 support by increase axon branching by disassembling actin microfilaments. CSPG stimulation
490 can increase axoplasmic Ca^{2+} (67, 68) and axoplasmic Ca^{2+} levels can determine which axonal
491 RNAs released from G3BP1 granules are translated through the phosphorylation of the
492 translation factor eIF2α in axons (20). Consistent with this, we find that *RhoA* mRNA
493 coprecipitates with neuronal G3BP1 protein and this interaction is decreased in the presence of
494 aggrecan but was not affected by the G3BP1 granule disassembling CPP. Interestingly, RhoA
495 activation was shown to increase formation of TIA1- and FMRP-containing stress granules in
496 other cellular systems (69), and CSPG-stimulated RhoA can activate the cytoplasmic histone
497 deacetylase HDAC6 in distal axons (68). Although Y27632 has been extensively used in the past
498 to inhibit ROCK, it is now known to inhibit multiple other kinases to some extent (70). So, we
499 cannot exclude the off-target effects of Y27632 contributing to the rescue in axon growth and
500 branching that we see in Fig. 4C-D. Deacetylation of G3BP1 lysine 376 by HDAC6 promotes
501 G3BP1 granule assembly (71). Considering that the rat 190-208 G3BP1 and human 191-209
502 sequences do not include the post-translationally modified Ser 149 or Lys 376, we suspect that
503 these CPPs do not alter post-translational modifications of G3BP1. Taken together, our data
504 raise the possibility that successful long-distance CNS axon regeneration with G3BP1 granule
505 inhibition will require simultaneous inhibition of RhoA.

506 In summary, our findings show that G3BP1 granules contribute to failed axon
507 regeneration after optic nerve and spinal cord injury. Thus, disassembly of G3BP1 granules, as
508 we have done here using G3BP1 B-domain expression or the 190-208 G3BP1 CPP, could bring a
509 new strategy to promote neural repair following brain and spinal cord injuries, either on their
510 own or strategically combined with other interventions. Importantly, the G3BP1 190-208 CPP
511 strategy used here is effective when delivered 2 days after PNS injury and at least 30 days after
512 spinal cord injury, which elevates the potential clinical relevance of these reagents for neural
513 repair treatments. Structure-activity relationship studies point to alternating acidic residue (Glu
514 or Asp) and Pro repeats as the functional component of the 190-208 G3BP1 CPP. This presents
515 opportunities for further refinement of the CPP activity, and since the 191-209 human G3BP1
516 CPP promotes axon growth in human iPSC-derived CNS neurons, we anticipate that similar
517 reagents may have high translational value for neural repair in human patients.

518 **MATERIALS AND METHODS**

519 ***Animal use –*** Institutional Animal Care and Use Committees of University of South Carolina,
520 Rutgers University, Boston Children's Hospital, Emory University, University of California San
521 Diego, Texas A&M University, and Drexel University approved all animal procedures. Sprague
522 Dawley rats (SD; 175-250 g) were used for sciatic nerve injury, and spinal cord injury, and wild
523 type 129s mice were used for optic nerve injury experiments. Survival surgery methods are
524 described below.

525 ***Peripheral nerve injury –*** For crush injury of the sciatic nerve, 5% isoflurane in 1 L/min oxygen
526 was used for anesthesia and maintained at 2% isoflurane in 1 L/min oxygen. Anesthetized rats or
527 mice were subjected to a manual crush at mid-thigh two times at 15 sec each using fine

528 jeweler's forceps with a 30 sec interval, and sciatic nerves were isolated 1 week later as
529 previously described (72).
530 ***Analysis of muscle reinnervation after peripheral nerve injury*** – Following nerve injury and
531 CPP injections, the extent of reinnervation of the hindlimb muscles was evaluated using in vivo
532 electromyography (EMG). Anesthesia was induced with 5% isoflurane in 1 L/min oxygen and
533 maintained at 2% isoflurane in 1 L/min oxygen.
534 ***Spinal cord injury stem cell graft*** – Adult female F344 Fischer rats received C4 dorsal column
535 lesion spinal cord injury. Surgeries were conducted under deep anesthesia using a combination
536 of ketamine (50 mg/kg), xylazine (2.6 mg/kg), and acepromazine (0.5 mg/kg). After performing a
537 laminectomy, a tungsten wire knife (McHugh Milieux, Downers Grove, IL) was positioned 0.6
538 mm lateral to the midline and inserted to a depth of 1 mm beneath the dorsal surface of the
539 spinal cord. The knife's arc was then extended 1.5 mm and elevated to transect the dorsal
540 columns as previously described (73). This injury model transects over 95% of corticospinal
541 axons (74).
542 ***Analysis of reticulospinal tract axon regeneration in PNGs*** – For testing expression of G3BP1
543 B-domain in reticulospinal neurons, AAV5-G3BP1-BFP or AAV5-B domain-BFP was microinjected
544 into the brainstem of female SD (225 g, obtained from Charles River) on day 1 of
545 experimentation. Control rats received AAV5-GFP. Rats received three 1 µl injections at 1 mm
546 rostral-caudal separations into medial-ventral gigantocellular areas of the reticular formation
547 (see Figure 1B).
548 ***Optic nerve injury and RGC survival analysis*** – Optic nerve regeneration and RGC survival were
549 investigated in 129s mice. The optic nerve was exposed and crushed 1-2 mm behind the orbit
550 using jeweler's forceps using methods that have been previously described (26, 75-77).

551 ***Cell culture*** – For primary neuronal cultures, DRGs were harvested in Hibernate-A medium
552 (BrainBits; Cordova, TN) and then dissociated as described (72). After centrifugation and
553 washing in DMEM/F12 (Life Technologies), dissociated ganglia were resuspended in DMEM/F12,
554 1 x N1 supplement (Sigma), 10% fetal bovine serum (Hyclone; Logan, UT), and 10 µM cytosine
555 arabinoside (Sigma). Dissociated DRGs were plated immediately on poly-L-lysine (Sigma) +
556 laminin (Sigma-Millipore, St. Louis, MO) or poly-L-lysine + aggrecan (R&D Systems, Minneapolis,
557 MN) coated surfaces (20, 72). For Schwann cells, dissociated DRGs were cultured as above
558 without cytosine arabinoside. Schwann cells were identified at 2 DIV by co-immunostaining for
559 GFAP in the puromycinylation studies. The use of human iPSCs was approved by the Institutional
560 Review Board at the University of South Carolina. Human iPSCs from apparently healthy euploid
561 individuals were obtained from Dr. Alberto Costa (Case Western Reserve University; Cleveland,
562 Ohio) (78).
563 ***Viral expression constructs*** – AAV2 and AAV5 preparations were generated in Vigene
564 Biosciences/Charles Rivers Labs (Wilmington, MA) and the viruses were titrated in DRG cultures
565 by incubating with 1.8-2.8 x 10^{10} particles of AAV2/5 overnight. Generation of the viral
566 constructs has been described previously (18).
567 ***Generation of Tat-tagged G3BP1 B domain peptides*** – Eight peptides were generated from the
568 rat G3BP1 B domain sequence (amino acids 140-220; UniProt ID # D3ZYS7_RAT) by Peptide 2.0
569 (Chantilly, VA) and Bachem Americas, Inc. (Torrance, CA).
570 ***Puromycinylation assays*** – At 2 DIV, Schwann cells were starved using DMEM/F12 and 1x L-
571 Glutamine for 3 h. 10 µM Scrambled or 192-205-CPPs were added 15 min before completion of
572 starvation. Schwann cells were stimulated with 10% FBS and 1x N1 supplement. For translation
573 inhibition controls, anisomycin (Sigma, 40 µM) or DMSO was added 30 min before completion of

574 starvation for a total duration of 45 min. Puromycin (Sigma, 2 µg/ml) was added at the time of
575 stimulation for a total duration of 15 min (79, 80). Cultures were then fixed with 4% PFA, and
576 immunofluorescence for GFAP and puromycin was performed.

577 ***RNA immunoprecipitation (RIP)*** **–** 10 DIV cultured rat cortical neurons were treated with PBS,
578 laminin (5 µg/ml), or aggrecan (5 µg/ml) in solution for 4 h were used for RIP studies. Neurons
579 were collected and washed twice with cold PBS and were lysed in RIP buffer (containing
580 100 mM KCl, 5 mM $MgCl_2$, 10 mM HEPES [pH 7.0], 1 mM DTT, and 0.5% NP-40 supplemented
581 with 1 × protease inhibitor cocktail (Roche) and RNasin Plus (Invitrogen), by pipetting up-down
582 and incubating on ice for 10 min. Lysate was cleared by centrifugation at 12,000×g for 20 min.
583 Pre-washed Protein A/G Dynabeads (ThermoFisher) were incubated at 4°C for 1 h with anti-
584 rabbit IgG (Jackson Immunoresearch) or anti-G3BP1 antibody (Fisher Scientific) at 0.67 µg/ml
585 each in RNAse-free PBS and then washed with RIP buffer three times. The antibody-bound
586 beads were resuspended with 500 µl of NT2 buffer (containing 50 mM Tris-HCl [pH 7.4],
587 150 mM NaCl, 1 mM $MgCl_2$ and 0.5% NP-40 supplemented with 1 × protease inhibitor cocktail
588 and RNasin Plus (Invitrogen). 10% of cleared lysate was kept as input, and the rest was divided
589 in half for control IgG RIP or G3BP1 RIP. Lysates were added to antibody-protein A/G beads
590 complex in NT2 buffer and incubated at 4°C for 4 h. The immunocomplexes were washed with
591 NT2 buffer 6 times (18). The bound RNAs were purified and analyzed by RTddPCR (*see below*).

592 ***RNA isolation and RT-ddPCR analysis*** **–** RNA was isolated from inputs and immunoprecipitates
593 using Trizol (Invitrogen) and chloroform (MP biomedicals) and subsequently precipitated using
594 isopropanol and washed with 75% ethanol. Reverse transcription was done using LunaScript®
595 RT SuperMix Kit (NEB). ddPCR products were detected using QX200™ ddPCR™ EvaGreen
596 Supermix (Biorad) and QX200™ droplet reader (Biorad).

597 Custom transcript-specific primer sets used for ddPCR were as follows: *RhoA*, forward
598 primer - CCAGACTGGACTGAGGAAATAG and reverse primer - GAAAGGAGCACTGTGACTTAGA;
599 *mTor*, forward primer - TGTCTGATTCTTACCACGCA and reverse primer -
600 CTCTTTGGCCAGGGTCTCAT; and *Pten*, forward primer - AGCGTGCGGATAATGACAAG and reverse
601 primer - GGATTTGATGGTTCCTCTACTG.

602 ***Immunoblotting*** **–** For immunoblotting, proteins were transferred from gels to nitrocellulose
603 membranes and blocked for 1 hour with 5% milk in Tris-buffered saline with 0.1% Tween 20
604 (TBST) at room temperature. Membranes were incubated overnight at 4°C with Rabbit anti-
605 G3BP1 antibody (1:2,000; Sigma) diluted in the blocking buffer while rocking. After washing with
606 TBST, membranes were incubated for 1 hour at room temperature with HRP-conjugated anti-
607 rabbit IgG secondary antibody (1:5,000; Jackson ImmunoResearch). Following washes with TBST,
608 immunocomplexes were visualized using Clarity™ Western ECL Substrate (Biorad).

609 ***Immunofluorescent staining*** **–** All procedures were performed at room temperature (RT)
610 unless specified otherwise. Cultured neurons were fixed in 4 % paraformaldehyde (PFA) in
611 phosphate-buffered saline (PBS), permeabilized in 0.3% TritonX, and incubated with primary and
612 secondary antibody solutions in blocking buffer as described previously (81).

613 ***Image analyses and processing*** **–** For analyses of stress granule protein levels in tissues, z
614 planes of the xyz scans of spinal cord sections were analyzed using *ImageJ*. Axons, neurons, and
615 Schwann cells were identified using specific markers, and SG protein colocalization with
616 neuronal or glial cell makers was assayed as described previously (14).

617 ***Statistical analyses*** **–** One-way ANOVA, Two-way ANOVA, or an equivalent non-parametric test
618 was used to compare means of > 2 independent groups and Student's *t*-test or Mann-Whitney
619 test was used to compare between 2 groups. p values of ≤ 0.05 were considered as statistically

significant. Z scores were calculated using the formula $\{\frac{x-\mu}{\sigma}\}$, where x = sample mean, μ = population mean, and σ = population standard deviation.

Other Methods – Detailed methods can be found in the *SI Appendix*, *Supplemental Materials and Methods*.

626 **Acknowledgements:** The authors thank members of the K. Welshhans, F. Poulain and D.S.
627 Smith laboratories at the University of South Carolina for constructive discussions. JL Twiss is
628 the incumbent SmartState Chair in Childhood Neurotherapeutics at the University of South
629 Carolina.

630 **Funding:** This work was supported by grants from the National Institutes of Neurological
631 Disorders and Stroke of the NIH (R01-NS0117821 to JLT, PW, AE, and JDH), the Dr. Miriam and
632 Sheldon G. Adelson Medical Research Foundation (to JLT, MT, and LB), the Craig H. Neilsen
633 Foundation (733151 to JLT and JND), the South Carolina Spinal Cord Injury Research Fund (to
634 PKS and JLT), the Merkin Peripheral Neuropathy and Nerve Regeneration Center (to PKS), and
635 the University of South Carolina Vice President for Research Office (JLT).

636 **Data and materials availability:** The data that support the findings of this study will be
637 deposited in a public repository (https://odc-sci.org). PKS and JLT hold a US patent on use of the
638 G3BP1 cell permeable peptide for axon regeneration and neurodegeneration. So, request for
639 this reagent will be available by materials transfer agreements (MTAs) with the University of
640 South Carolina.
641

642 **REFERENCES**

643 1. A. Hoke, Mechanisms of Disease: what factors limit the success of peripheral nerve
644 regeneration in humans? *Nature clinical practice. Neurology* **2**, 448-454 (2006).

645 2. J. W. Fawcett, The Struggle to Make CNS Axons Regenerate: Why Has It Been so
646 Difficult? *Neurochem Res* **45**, 144-158 (2020).

647 3. Y. Ohtake *et al.*, The effect of systemic PTEN antagonist peptides on axon growth and
648 functional recovery after spinal cord injury. *Biomaterials* **35**, 4610-4626 (2014).

649 4. N. Abe, S. H. Borson, M. J. Gambello, F. Wang, V. Cavalli, mTOR activation increases
650 axonal growth capacity of injured peripheral nerves. *J Biol Chem* **285**, 28034-28043
651 (2010).

652 5. K. J. Christie, C. A. Webber, J. A. Martinez, B. Singh, D. W. Zochodne, PTEN inhibition to
653 facilitate intrinsic regenerative outgrowth of adult peripheral axons. *J Neurosci* **30**, 9306-
654 9315 (2010).

655 6. C. A. Danilov, O. Steward, Conditional genetic deletion of PTEN after a spinal cord injury
656 enhances regenerative growth of CST axons and motor function recovery in mice. *Exp*
657 *Neurol* **266**, 147-160 (2015).

658 7. K. Liu *et al.*, PTEN deletion enhances the regenerative ability of adult corticospinal
659 neurons. *Nat Neurosci* **13**, 1075-1081 (2010).

660 8. K. K. Park, K. Liu, Y. Hu, J. L. Kanter, Z. He, PTEN/mTOR and axon regeneration.
661 *Experimental Neurology* **223**, 45-50 (2010).

662 9. K. K. Park *et al.*, Promoting axon regeneration in the adult CNS by modulation of the
663 PTEN/mTOR pathway. *Science* **322**, 963-966 (2008).

664 10. T. P. Smith, P. K. Sahoo, A. N. Kar, J. L. Twiss, Intra-axonal mechanisms driving axon
665 regeneration. *Brain Res* **1740**, 146864 (2020).

666 11. H. H. Wong *et al.*, RNA Docking and Local Translation Regulate Site-Specific Axon
667 Remodeling In Vivo. *Neuron* **95**, 852-868 e858 (2017).

668 12. T. Shigeoka *et al.*, Dynamic Axonal Translation in Developing and Mature Visual Circuits.
669 *Cell* **166**, 181-192 (2016).

670 13. H. Jung, B. C. Yoon, C. E. Holt, Axonal mRNA localization and local protein synthesis in
671 nervous system assembly, maintenance and repair. *Nature reviews. Neuroscience* **13**,
672 308-324 (2012).

673 14. A. L. Kalinski *et al.*, mRNAs and Protein Synthetic Machinery Localize into Regenerating
674 Spinal Cord Axons When They Are Provided a Substrate That Supports Growth. *J*
675 *Neurosci* **35**, 10357-10370 (2015).

676 15. B. A. Walker *et al.*, Reprogramming axonal behavior by axon-specific viral transduction.
677 *Gene therapy* **19**, 947-955 (2012).

678 16. R. Sachdeva, K. Farrell, M. K. McMullen, J. L. Twiss, J. D. Houle, Dynamic Changes in Local
679 Protein Synthetic Machinery in Regenerating Central Nervous System Axons after Spinal
680 Cord Injury. *Neural plasticity* **2016**, 4087254 (2016).

681 17. D. E. Willis *et al.*, Axonal Localization of transgene mRNA in mature PNS and CNS
682 neurons. *J Neurosci* **31**, 14481-14487 (2011).

683 18. P. K. Sahoo *et al.*, Axonal G3BP1 stress granule protein limits axonal mRNA translation
684 and nerve regeneration. *Nat Commun* **9**, 3358 (2018).

685 19. P. Anderson, N. Kedersha, RNA granules: post-transcriptional and epigenetic modulators
686 of gene expression. *Nat Rev Mol Cell Biol* **10**, 430-436 (2009).

687 20. P. Sahoo *et al.*, A translational switch drives axonal stress granule disassembly through
688 Casein Kinase 2α. *Curr Biol* **30**, 4882-4895.E4886 (2020).

689 21. P. Lu *et al.*, Long-distance growth and connectivity of neural stem cells after severe
690 spinal cord injury. *Cell* **150**, 1264-1273 (2012).

691 22. J. F. Bonner *et al.*, Grafted Neural Progenitors Integrate and Restore Synaptic
692 Connectivity across the Injured Spinal Cord. *J Neurosci* **31**, 4675-4686 (2011).

693 23. N. M. Tran *et al.*, Single-Cell Profiles of Retinal Ganglion Cells Differing in Resilience to
694 Injury Reveal Neuroprotective Genes. *Neuron* **104**, 1039-1055 e1012 (2019).

695 24. E. R. Bray *et al.*, Thrombospondin-1 Mediates Axon Regeneration in Retinal Ganglion
696 Cells. *Neuron* **103**, 642-657 e647 (2019).

697 25. Y. Hu *et al.*, Differential effects of unfolded protein response pathways on axon injury-
698 induced death of retinal ganglion cells. *Neuron* **73**, 445-452 (2012).

699 26. S. Leon, Y. Yin, J. Nguyen, N. Irwin, L. I. Benowitz, Lens injury stimulates axon
700 regeneration in the mature rat optic nerve. *J Neurosci* **20**, 4615-4626 (2000).

701 27. D. S. Smith, P. Skene, A transcription-dependent switch controls competence of adult
702 neurons for distinct modes of axon growth. *J. Neurosci.* **17**, 646-658. (1997).

703 28. J. Q. Zheng *et al.*, A functional role for intra-axonal protein synthesis during axonal
704 regeneration from adult sensory neurons. *J Neurosci* **21**, 9291-9303 (2001).

705 29. D. Vuppalanchi *et al.*, Conserved 3'-untranslated region sequences direct subcellular
706 localization of chaperone protein mRNAs in neurons. *J Biol Chem* **285**, 18025-18038
707 (2010).

708 30. S. Stern *et al.*, RhoA drives actin compaction to restrict axon regeneration and astrocyte
709 reactivity after CNS injury. *Neuron* **109**, 3436-3455 e3439 (2021).

710 31. B. A. Walker, S. J. Ji, S. R. Jaffrey, Intra-axonal translation of RhoA promotes axon growth
711 inhibition by CSPG. *J Neurosci* **32**, 14442-14447 (2012).

712 32. J. Ng *et al.*, Rac GTPases control axon growth, guidance and branching. *Nature* **416**, 442-
713 447 (2002).

714 33. S. Tivodar *et al.*, Rac-GTPases Regulate Microtubule Stability and Axon Growth of
715 Cortical GABAergic Interneurons. *Cereb Cortex* **25**, 2370-2382 (2015).

716 34. S. J. Lee *et al.*, Selective axonal translation of the mRNA isoform encoding prenylated
717 Cdc42 supports axon growth. *J Cell Sci* **134** (2021).

718 35. M. L. Pearn *et al.*, Inhibition of RhoA reduces propofol-mediated growth cone collapse,
719 axonal transport impairment, loss of synaptic connectivity, and behavioural deficits. *Br J*
720 *Anaesth* **120**, 745-760 (2018).

721 36. R. E. Gross, Q. Mei, C. A. Gutekunst, E. Torre, The pivotal role of RhoA GTPase in the
722 molecular signaling of axon growth inhibition after CNS injury and targeted therapeutic
723 strategies. *Cell Transplant* **16**, 245-262 (2007).

724 37. M. A. Kopp *et al.*, Small-molecule-induced Rho-inhibition: NSAIDs after spinal cord
725 injury. *Cell Tissue Res* **349**, 119-132 (2012).

726 38. J. F. Borisoff *et al.*, Suppression of Rho-kinase activity promotes axonal growth on
727 inhibitory CNS substrates. *Mol Cell Neurosci* **22**, 405-416 (2003).

728 39. E. M. Hur *et al.*, Engineering neuronal growth cones to promote axon regeneration over
729 inhibitory molecules. *Proc Natl Acad Sci U S A* **108**, 5057-5062 (2011).

730 40. J. Wojnacki *et al.*, Dual spatio-temporal regulation of axon growth and microtubule
731 dynamics by RhoA signaling pathways. *J Cell Sci* **137** (2024).

732 41. M. G. Andrusiak *et al.*, Inhibition of Axon Regeneration by Liquid-like TIAR-2 Granules.
733 *Neuron* **104**, 290-304 (2019).

734 42. S. Neumann, C. J. Woolf, Regeneration of dorsal column fibers into and beyond lesion
735 site following adult spinal cord injury. *Neuron* **23**, 83-91 (1999).

736 43. L. I. Benowitz, L. Xie, Y. Yin, Inflammatory Mediators of Axon Regeneration in the Central
737 and Peripheral Nervous Systems. *Int J Mol Sci* **24** (2023).

738 44. J. Yang, Y. Yin, PTEN in Chromatin Remodeling. *Cold Spring Harb Perspect Med* **10**
739 (2020).

740 45. J. O. Lipton, M. Sahin, The neurology of mTOR. *Neuron* **84**, 275-291 (2014).

741 46. M. Terenzio *et al.*, Locally translated mTOR controls axonal local translation in nerve
742 injury. *Science* **359**, 1416-1421 (2018).

743 47. M. J. Kye *et al.*, SMN regulates axonal local translation via miR-183/mTOR pathway.
744 *Human molecular genetics* **23**, 6318-6331 (2014).

745 48. A. Poulopoulos *et al.*, Subcellular transcriptomes and proteomes of developing axon
746 projections in the cerebral cortex. *Nature* **565**, 356-360 (2019).

747 49. P. Yang *et al.*, G3BP1 Is a Tunable Switch that Triggers Phase Separation to Assemble
748 Stress Granules. *Cell* **181**, 325-345 e328 (2020).

749 50. C. UniProt, UniProt: the Universal Protein Knowledgebase in 2023. *Nucleic Acids Res* **51**,
750 D523-D531 (2023).

751 51. J. Guillen-Boixet *et al.*, RNA-Induced Conformational Switching and Clustering of G3BP
752 Drive Stress Granule Assembly by Condensation. *Cell* **181**, 346-361 e317 (2020).

753 52. K. Stillger, I. Neundorf, Cell-permeable peptide-based delivery vehicles useful for
754 subcellular targeting and beyond. *Cell Signal* **109**, 110796 (2023).

755 53. N. Lev *et al.*, A DJ-1 Based Peptide Attenuates Dopaminergic Degeneration in Mice
756 Models of Parkinson's Disease via Enhancing Nrf2. *PLoS One* **10**, e0127549 (2015).

757 54. C. Marelli, F. Maschat, The P42 peptide and Peptide-based therapies for Huntington's
758 disease. *Orphanet J Rare Dis* **11**, 24 (2016).

759 55. S. Elmsaouri, S. Markmiller, G. W. Yeo, APEX Proximity Labeling of Stress Granule
760 Proteins. *Methods Mol Biol* **2428**, 381-399 (2022).

761 56. S. Hu *et al.*, Time-resolved proteomic profiling reveals compositional and functional
762 transitions across the stress granule life cycle. *Nat Commun* **14**, 7782 (2023).

763 57. H. Marmor-Kollet *et al.*, Spatiotemporal Proteomic Analysis of Stress Granule
764 Disassembly Using APEX Reveals Regulation by SUMOylation and Links to ALS
765 Pathogenesis. *Mol Cell* **80**, 876-891.e876 (2020).

766 58. T. Altman *et al.*, Axonal TDP-43 condensates drive neuromuscular junction disruption
767 through inhibition of local synthesis of nuclear encoded mitochondrial proteins. *Nat*
768 *Commun* **12**, 6914 (2021).

769 59. Y. C. Liao *et al.*, RNA Granules Hitchhike on Lysosomes for Long-Distance Transport,
770 Using Annexin A11 as a Molecular Tether. *Cell* **179**, 147-164 e120 (2019).

771 60. A. Lamiable *et al.*, PEP-FOLD3: faster de novo structure prediction for linear peptides in
772 solution and in complex. *Nucleic Acids Res* **44**, W449-454 (2016).

773 61. Y. Shen, J. Maupetit, P. Derreumaux, P. Tuffery, Improved PEP-FOLD Approach for
774 Peptide and Miniprotein Structure Prediction. *J Chem Theory Comput* **10**, 4745-4758
775 (2014).

776 62. P. Thevenet *et al.*, PEP-FOLD: an updated de novo structure prediction server for both
777 linear and disulfide bonded cyclic peptides. *Nucleic Acids Res* **40**, W288-293 (2012).

778 63. Y. Fujita, T. Yamashita, Axon growth inhibition by RhoA/ROCK in the central nervous
779 system. *Frontiers in neuroscience* **8**, 338 (2014).

780 64. K. Y. Wu *et al.*, Local translation of RhoA regulates growth cone collapse. *Nature* **436**,
781 1020-1024 (2005).

782 65. S. P. Somasekharan *et al.*, G3BP1-linked mRNA partitioning supports selective protein
783 synthesis in response to oxidative stress. *Nucleic Acids Res* **48**, 6855-6873 (2020).

784 66. E. W. Dent, K. Kalil, Axon branching requires interactions between dynamic
785 microtubules and actin filaments. *J Neurosci* **21**, 9757-9769 (2001).

786 67. D. M. Snow, P. B. Atkinson, T. D. Hassinger, P. C. Letourneau, S. B. Kater, Chondroitin
787 sulfate proteoglycan elevates cytoplasmic calcium in DRG neurons. *Developmental*
788 *biology* **166**, 87-100 (1994).

789 68. A. L. Kalinski *et al.*, Deacetylation of Miro1 by HDAC6 blocks mitochondrial transport and
790 mediates axon growth inhibition. *J Cell Biol* **218**, 1871-1890 (2019).

791 69. N. P. Tsai, L. N. Wei, RhoA/ROCK1 signaling regulates stress granule formation and
792 apoptosis. *Cell Signal* **22**, 668-675 (2010).

793 70. T. Anastassiadis, S. W. Deacon, K. Devarajan, H. Ma, J. R. Peterson, Comprehensive assay
794 of kinase catalytic activity reveals features of kinase inhibitor selectivity. *Nat Biotechnol*
795 **29**, 1039-1045 (2011).

796 71. J. Gal *et al.*, The Acetylation of Lysine-376 of G3BP1 Regulates RNA Binding and Stress
797 Granule Dynamics. *Mol Cell Biol* **39**, e00052-00019 (2019).

798 72. J. L. Twiss, D. S. Smith, B. Chang, E. M. Shooter, Translational control of ribosomal
799 protein L4 mRNA is required for rapid neurite regeneration. *Neurobiology of disease* **7**,
800 416-428 (2000).

801 73. J. N. Dulin *et al.*, Injured adult motor and sensory axons regenerate into appropriate
802 organotypic domains of neural progenitor grafts. *Nat Commun* **9**, 84 (2018).

803 74. N. Weidner, A. Ner, N. Salimi, M. H. Tuszynski, Spontaneous corticospinal axonal
804 plasticity and functional recovery after adult central nervous system injury. *Proc Natl*
805 *Acad Sci U S A* **98**, 3513-3518 (2001).

806 75. Y. Yin *et al.*, Oncomodulin is a macrophage-derived signal for axon regeneration in
807 retinal ganglion cells. *Nat Neurosci* **9**, 843-852 (2006).

808 76. S. de Lima *et al.*, Full-length axon regeneration in the adult mouse optic nerve and
809 partial recovery of simple visual behaviors. *Proc Natl Acad Sci U S A* **109**, 9149-9154
810 (2012).

811 77. L. Xie *et al.*, Monocyte-derived SDF1 supports optic nerve regeneration and alters retinal
812 ganglion cells' response to Pten deletion. *Proc Natl Acad Sci U S A* **119**, e2113751119
813 (2022).

814 78. M. L. Y, B. L. Zampieri, J. J. Scott-McKean, M. W. Johnson, A. C. S. Costa, Generation of
815 Integration-Free Induced Pluripotent Stem Cells from Urine-Derived Cells Isolated from
816 Individuals with Down Syndrome. *Stem cells translational medicine* **6**, 1465-1476 (2017).

817 79. J.-M. Cioni *et al.*, Late Endosomes Act as mRNA Translation Platforms and Sustain
818 Mitochondria in Axons. *Cell* **176**, 56-72.e15 (2019).

819 80. A.-S. Hafner, P. G. Donlin-Asp, B. Leitch, E. Herzog, E. M. Schuman, Local protein
820 synthesis is a ubiquitous feature of neuronal pre- and postsynaptic compartments.
821 *Science* **364**, eaau3644 (2019).

822 81. T. T. Merianda, C. Gomes, S. Yoo, D. Vuppalanchi, J. L. Twiss, Axonal localization of
823 neuritin/CPG15 mRNA in neuronal populations through distinct 5' and 3' UTR elements.
824 *J Neurosci* **33**, 13735-13742 (2013).

825

826

827 **MAIN FIGURES**

828

829 **Figure 1**: ***Expression of G3BP1 acidic domain in CNS neurons facilitates axon regeneration.***

830 ***A,*** Representative exposure-matched confocal images of corticospinal axons in spinal cord

831 labeled with biotinylated dextran amine (BDA) following C4 level contusion injury and

832 subsequent grafting with rostralized or caudalized stem cell graft (21). Upper row shows XY

833 optical plane through CST axon regenerating into graft; lower row shows signals for stress

834 granule proteins G3BP1 and TIA1 that overlap with BDA across Z sections as XYZ projection in a

835 separate channel ('axonal G3BP1 + TIA1'). There are stress granules present in the few axons

836 regenerating into rostralized grafts, and these are absent in the more numerous axons

837 regenerating into caudalized grafts [scale bar = 10 µm].

838 ***B,*** Schematic of experimental paradigm and timeline for spinal cord injury model used in C-D,

839 with regeneration of reticulospinal neurons in the permissive environment of a peripheral nerve

840 graft (PNG).

841 ***C,*** Exposure-matched epifluorescence images for NF- + βIII Tubulin-immunostained PNGs from

842 animals transduced with AAV5-GFP, -G3BP1-BFP, or -G3BP1 B domain-BFP shown at indicated

843 distances from grafting site at proximal side of transected spinal cord. For G3BP1 granule size

844 and density after CPP treatment see Supplemental Figure S1A-C [scale bar = 500 µm].

845 ***D,*** Quantitation of regenerating reticulospinal axon profile numbers in PNGs from panel C at

846 indicated distances away from grafting site in spinal cord shown as mean ± standard error of the

847 mean (SEM; N = 5 animals; *$p \leq 0.05$ vs. GFP- and & $p \leq 0.05$ vs. G3BP1-BFP by two-way

848 ANOVA with Tukey HSD post-hoc).

849 ***E,*** Schematic of experimental paradigm for AAV transduction of retinal ganglion cells (RGC) and

850 optic nerve crush injury used in F-G.

851 ***F,*** Confocal montage images of optic nerves for AAV2-GFP, -G3BP1-BFP, G3BP1 B-domain-BFP
852 transduced animals at 14 days post injury. Regenerating axons are detected by anti-GAP43 (red)
853 and GFP, G3BP1-BFP and G3BP1 B-domain-BFP signals by anti-BFP/GFP antibodies (green). For
854 G3BP1 granule size and density after CPP treatment see Supplemental Figure S1D-F [scale bar =
855 250 μm].
856 ***G,*** Quantitation of GAP43 signals from F for regenerating RGC axon profiles is shown as mean ±
857 SEM (N ≥ 5 animals; **p ≤ 0.01 and ****p ≤ 0.0001 vs. GFP- and && p ≤ 0.01 and &&&& p ≤
858 0.001 vs. G3BP1-BFP-transduced animals by two-way ANOVA with Tukey HSD post-hoc). For
859 RGC survival data see Supplemental Figure S2.
860
861 **Figure 2**: ***G3BP1 190-208 peptide promotes PNS and CNS axon growth.***
862 ***A,*** Schematic of rat G3BP1 protein with defined domains shown on the top. Sequence of acidic
863 domain (B domain) of G3BP1 shown below with sequence of amino acids 147-166, 168-189 and
864 190-208 used for cell permeable peptides (CPP). Variants of these CPPs tested in panels F-G and
865 Supplemental Figures S3-4 are indicated.
866 ***B,*** Timeline for sciatic nerve injury followed by intra-nerve G3BP1 CPP treatments used for
867 panels C-E and Supplemental Figure S3A.
868 ***C-D,*** Exposure-matched epifluorescence images for anti-SCG10 immunostained sciatic nerves 7
869 days post-crush that were treated with indicated CPPs or PBS are shown in **C**. Dotted line shows
870 the injury site. Quantitation of SCG10+ axon profiles at indicated distances past the injury site
871 from C is shown in **D** as mean ± SEM (N ≥ 6 animals; * p ≤ 0.05 by two-way ANOVA vs. 168-189
872 with Tukey HSD post-hoc) [scale bar = 500 μm].
873 ***E,*** Compound muscle action potentials (CMAP) are shown for gastrocnemius muscle of animals
874 treated with G3BP1 CPPs after sciatic nerve crush injury as in B are shown as average % intact M

875 responses ± SEM for indicated times (N ≥ 4 animals; *p≤0.05 by Student's t-test for indicated
876 data pairs). For CMAP data on tibialis anterior muscle see Supplemental Figure S3A.
877 ***F,*** Quantitation of total axon growth of cultured adult rat sensory (DRG) neurons treated with
878 G3BP1 CPP and variants is shown as mean ± SEM (left Y-axis) and Z score relative to population
879 mean (right Y-axis; N ≥ 352 neurons across three biological replicates for each condition; * p ≤
880 0.05 and **** p ≤ 0.0001 vs. 168-189 CPP by one-way ANOVA with Dunnett post-hoc).
881 Representative images and data on longest axon per neuron and branch density are shown in
882 Supplemental Figure S3.
883 ***G,*** Quantitation of total neurite length for human iPSC (hiPSC)-derived glutamatergic neurons
884 untreated (Sham) or treated with indicated G3BP1 CPPs and variants shown as mean ± SEM (left
885 Y-axis) and Z score vs. population mean (right Y-axis; N ≥ 1165 neurons across three biological
886 replicates for each condition; **** p ≤ 0.0001 vs. Sham by one-way ANOVA with Tukey HSD
887 post-hoc). Representative images plus longest neurite length and neurite branching data are
888 shown in Supplemental Figure S4.
889
890 **Figure 3**: ***G3BP1 190-208 cell permeable peptide promotes in vivo CNS axon regeneration.***
891 ***A,*** Schematic of experimental paradigm for spinal cord injury plus PNG and CPP treatment into
892 spinal cord just rostral to injury site used in B-D.
893 ***B,*** Quantitation of regenerating CNS axon profiles into PNGs from panel B at indicated distances
894 from spinal cord shown as mean ± SEM (N = 5 animals; *p≤0.05 by Student's t-test for
895 indicated data pairs).
896 ***C,*** Neurolucida tracing images for NF- + -βIII tubulin-immunostained regenerating axons in
897 proximal PNG shown. Primary branches are pseudo-colored as cyan and secondary/tertiary
898 branches are pseudo- colored from violet-to-magenta. Note increased violet to magenta

899 neurites in the G3BP1 190-208 CPP- vs. 168-189 CPP-treated animals indicating increased

900 branching [scale bar = 250 µm in large images and 25 µm in insets].

901 ***D,*** Quantitation of axonal branching from Neurolucida tracing from C shown as mean ± SEM (N =

902 5 animals; *p ≤ 0.05 by Student's t-test).

903 ***E,*** Schematic of experimental paradigm for spinal cord injury plus PNG and CPP treatment into

904 the PNG used in F-G is shown.

905 ***F,*** Representative fluorescent images show anti-SCG10 immunosignals for regenerating CNS

906 axons in PNGs. Yellow dotted line shows the junction between PNG and spinal cord, with many

907 more axons penetrating the spinal cord in G3BP1 190-208 CPP- than scrambled 190-208 (Scr

908 190-208 [E_7P_7])-treated animals [scale bar = 50 µm].

909 ***G,*** Quantitation of distal spinal cord reticulospinal axons from F shown as mean ± SEM (N = 6

910 animals; ***p ≤ 0.001 by Student's t-test).

911

912 **Figure 4**: ***G3BP1 acidic domain inhibits axonal G3BP1 granule assembly to enable CNS axon***

913 ***regeneration.***

914 ***A-B,*** Axon and dendrite length and branching for G3BP1 190-208 vs. 168-189 CPP-treated E18

915 rat cortical neurons cultured on growth-permissive (**A**; PDL) vs. growth-inhibitory (**B**; PDL +

916 aggrecan) substrates is shown as mean ± SEM. Note that axon and dendrite branching are

917 significantly increased on the growth inhibitory substrates with 190-208 CPP exposure (N ≥ 1042

918 neurons across 3 culture preparations for each condition; **** p ≤ 0.0001 by students T-test).

919 Axon morphologies for adult DRG cultured on aggrecan plus G3BP1 190-208 vs. 168-189 CPP

920 shown in Supplemental Figure S5C-D.

921 ***C,*** Representative epifluorescence images of SMI312 immunostained E18 rat cortical neurons

922 cultured on aggrecan and treated with G3BP1 190-208 CPP vs. scrambled 190-208 CPP ± 10 µM

923 RhoA kinase inhibitor shown [scale bar = 50 µm].

924 ***D,*** Quantitation of axon length and branching density for E18 cortical neurons as in C shown as

925 mean ± SEM (N ≥ 259 neurons across three repetitions for each condition; ****/&&&&

926 p ≤ 0.0001 by one-way ANOVA with Tukey HSD post-hoc; * for indicated treatment group vs.

927 scrambled 190-208-DMSO, & for indicated treatment group vs. 190-208-DMSO). Average length

928 axons extend beyond soma shown in Supplemental Figure S5E.

929

930 **<u>Figure 5</u>: *G3BP1 granule disassembling CPP affects other stress granule proteins, activates***

931 ***axonal protein synthesis, and shows specificity for mRNA release.***

932 ***A-C,*** Representative exposure-matched confocal images of axons of embryonic rat cortical

933 neurons labeled with axonal neurofilament marker SMI312 and G3BP1 are shown (**A**). The upper

934 panel of each image pair shows merged signals in a single XY plane, and the lower panel shows

935 the XYZ projection of G3BP1 signals that overlap with SMI312 across individual Z sections.

936 Quantitation of the density (**B**) and size (**C**) of axonal G3BP1 granules shown as mean ± SEM (**C**)

937 (N ≥ 33 axons across three biological replicates, ****p ≤ 0.0001 by Mann Whitney U test in B

938 and N ≥ 79 granules across three biological replicates, *p ≤ 0.05 by Mann Whitney U test in C)

939 [scale bar = 5 µm].

940 ***D-F,*** Representative exposure-matched confocal images of axons of embryonic rat cortical

941 neurons labeled with axonal neurofilament marker SMI312 and G3BP2 (**D**) are shown as in A.

942 Quantitation of the density (**E**) and size (**F**) of axonal G3BP2 granules shown as mean ± SEM (N ≥

943 38 axons across three biological replicates, ***p ≤ 0.001 by Mann Whitney U test in E and N ≥ 76

944 granules across three biological replicates, p values by Mann Whitney U test in F). For FMRP and
945 FXR1 granule size after CPP treatment, see Supplemental Figures S6A-F [scale bar = 5 μm].

946 ***G-I***, Exposure-matched epifluorescence images for SMI312 + Puromycin immunostained
947 embryonic rat cortical neurons after CPP treatment are shown (**G**). Quantitation of the amount
948 of puromycin in soma (**H**) and axons (**I**) of embryonic rat cortical neurons after CPP treatment
949 shown as mean ± SEM (N ≥ 28 neurons across three biological replicates; ****p ≤ 0.0001, **p ≤
950 0.01, *p ≤ 0.05 Kruskal Wallis test with Dunn's multiple comparisons). For puromycin
951 quantitation in Schwann cells after CPP treatment, see Supplemental Figures S6G, H [scale bar =
952 5 μm].

953 ***J-M,*** Schematic of experimental paradigm for analyses of RNAs coprecipitating with G3BP1 (**J**).
954 Quantitation of fold change in mRNA levels of *Rhoa* (**K**), *mTor* (**L**), and *Pten* (**M**) interacting with
955 G3BP1 after bath-application of laminin or aggrecan ± CPP treatment shown as mean ± SEM (N ≥
956 3 animals, *p ≤ 0.05, **p ≤ 0.01 by Ordinary One-way ANOVA with Dunnett's multiple
957 comparisons).

958

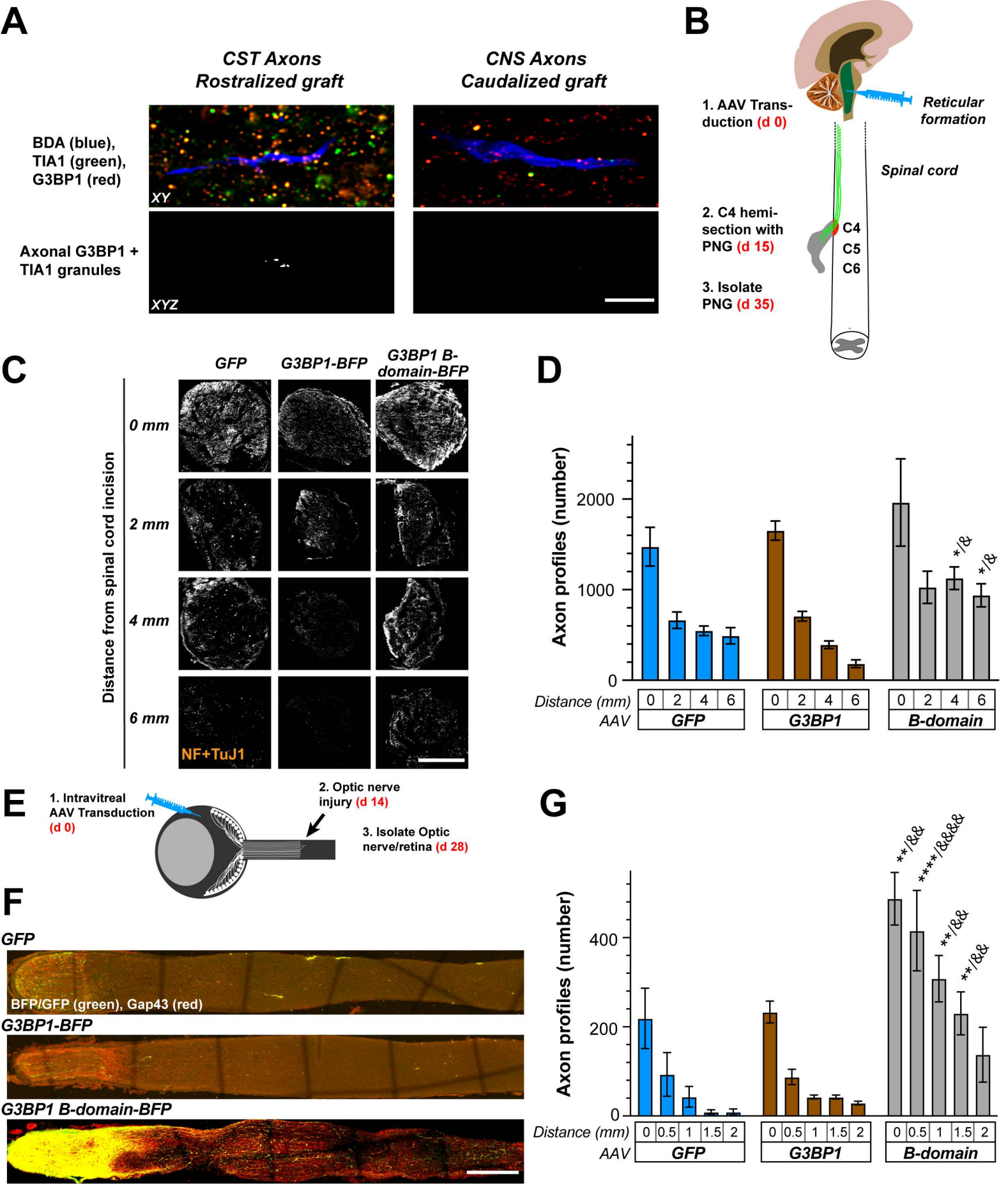
A
CST Axons
Rostralized graft
CNS Axons
Caudalized graft
BDA (blue),
TIA1 (green),
G3BP1 (red)
XY
Axonal G3BP1 +
TIA1 granules
XYZ
B
1. AAV Trans-
duction (d 0)
Reticular
formation
Spinal cord
2. C4 hemi-
section with
PNG (d 15)
C4
C5
C6
3. Isolate
PNG (d 35)
C
GFP
G3BP1-BFP
G3BP1 B-
domain-BFP
Distance from spinal cord incision
0 mm
2 mm
4 mm
6 mm
NF+TuJ1
D
Axon profiles (number)
2000
1000
0
*/&
*/&
Distance (mm)
0 2 4 6
0 2 4 6
0 2 4 6
AAV
GFP
G3BP1
B-domain
E
1. Intravitreal
AAV Transduction
(d 0)
2. Optic nerve
injury (d 14)
3. Isolate Optic
nerve/retina (d 28)
F
GFP
BFP/GFP (green), Gap43 (red)
G3BP1-BFP
G3BP1 B-domain-BFP
G
Axon profiles (number)
400
200
0
**/&&
****/&&&&
**/&&
**/&&
Distance (mm)
0 0.5 1 1.5 2
0 0.5 1 1.5 2
0 0.5 1 1.5 2
AAV
GFP
G3BP1
B-domain

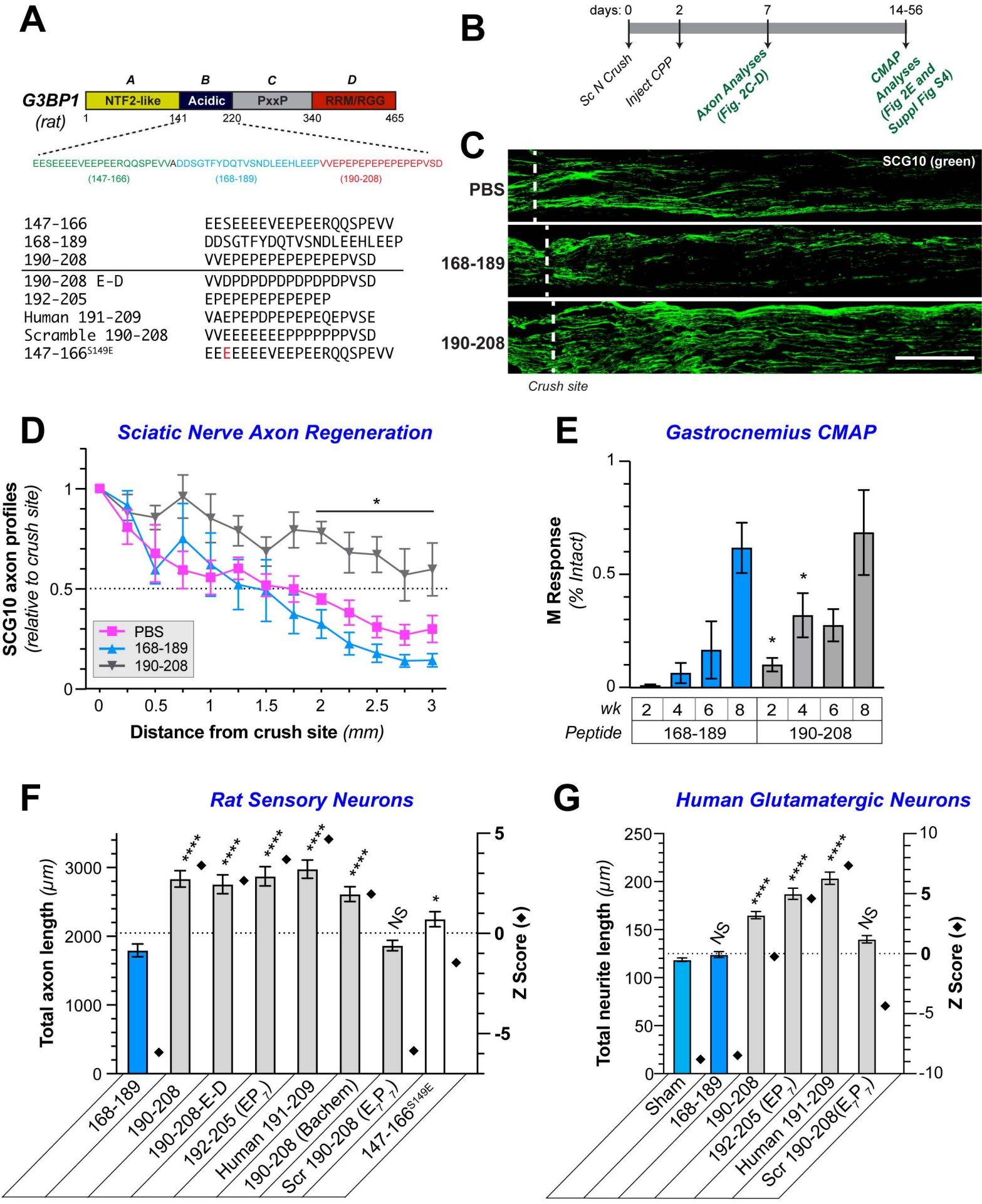
A
G3BP1
(rat)
A
B
C
D
NTF2-like
Acidic
PxxP
RRM/RGG
1
141
220
340
465
EESEEEEVEEPEERQQSPEVVADDSGTFYDQTVSNDLEEHLEEPVVEPEPEPEPEPEPVSD
(147-166)
(168-189)
(190-208)
147-166 EESEEEEVEEPEERQQSPEVV
168-189 DDSGTFYDQTVSNDLEEHLEEP
190-208 VVEPEPEPEPEPEPEPVSD
190-208 E-D VVDPDPDPDPDPDPDPVSD
192-205 EPEPEPEPEPEPEP
Human 191-209 VAEPEPDPEPEPEQEPVSE
Scramble 190-208 VVEEEEEEEPPPPPPPVSD
147-166S149E EEEEEEEVEEPEERQQSPEVV
B
days: 0
2
7
14-56
Sc N Crush
Inject CPP
Axon Analyses (Fig. 2C-D)
CMAP Analyses (Fig 2E and Suppl Fig S4)
C
SCG10 (green)
PBS
168-189
190-208
Crush site
D
Sciatic Nerve Axon Regeneration
SCG10 axon profiles (relative to crush site)
Distance from crush site (mm)
PBS
168-189
190-208
E
Gastrocnemius CMAP
M Response (% Intact)
wk
Peptide
168-189
190-208
F
Rat Sensory Neurons
Total axon length (μm)
Z Score (◆)
168-189
190-208
190-208-E-D
192-205 (EP7)
Human 191-209
190-208 (Bachem)
Scr 190-208 (E7P7)
147-166S149E
G
Human Glutamatergic Neurons
Total neurite length (μm)
Z Score (◆)
Sham
168-189
190-208
192-205 (EP7)
Human 191-209
Scr 190-208(E7P7)

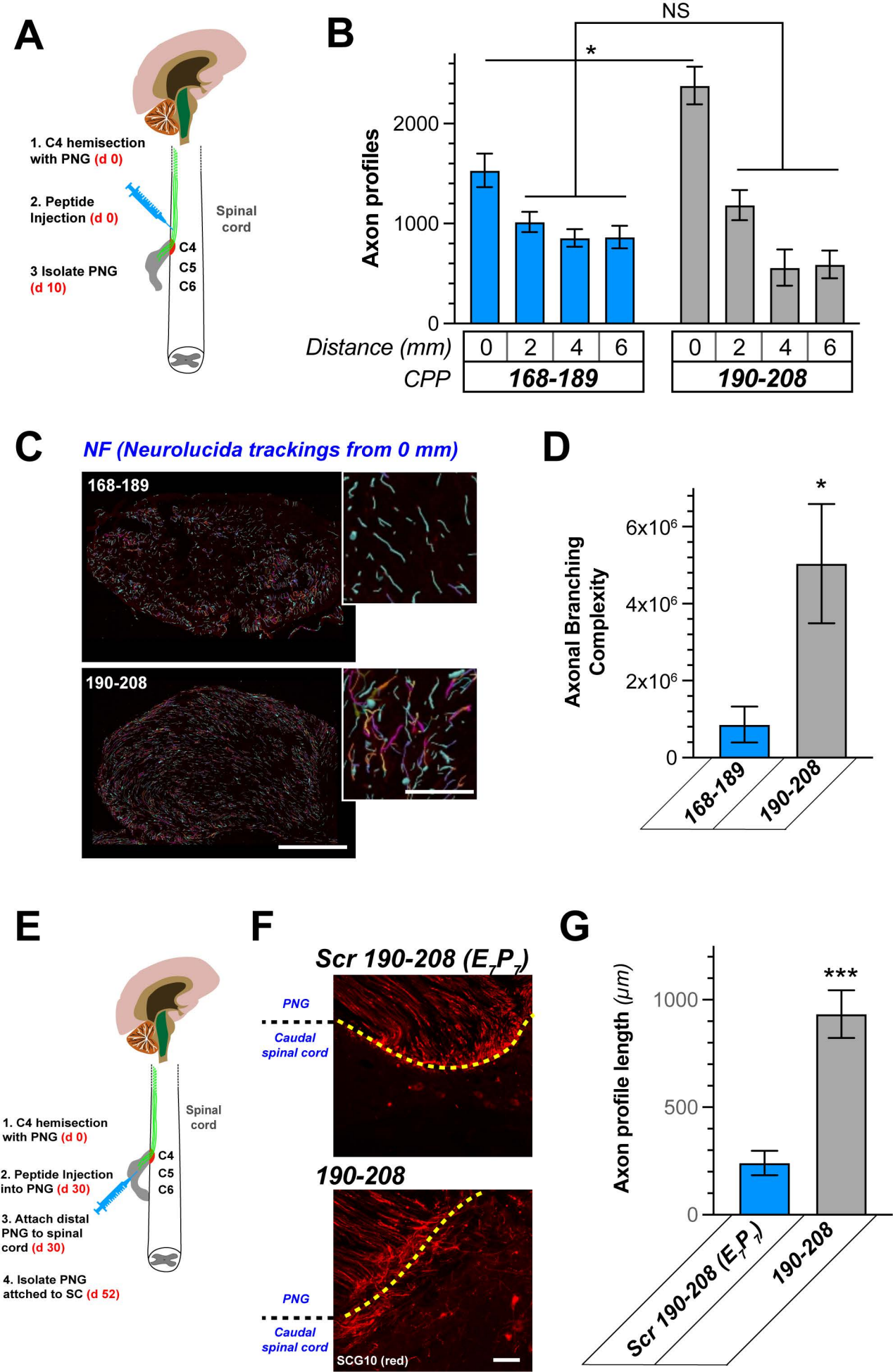
A
1. C4 hemisection with PNG (d 0)
2. Peptide Injection (d 0)
3 Isolate PNG (d 10)
Spinal cord
C4
C5
C6
B
NS
*
Axon profiles
2000
1000
0
Distance (mm)
0 2 4 6
0 2 4 6
CPP
168-189
190-208
C
NF (Neurolucida trackings from 0 mm)
168-189
190-208
D
*
Axonal Branching Complexity
6x10⁶
4x10⁶
2x10⁶
0
168-189
190-208
E
1. C4 hemisection with PNG (d 0)
2. Peptide Injection into PNG (d 30)
3. Attach distal PNG to spinal cord (d 30)
4. Isolate PNG attched to SC (d 52)
Spinal cord
C4
C5
C6
F
Scr 190-208 (E7P7)
PNG
Caudal spinal cord
190-208
PNG
Caudal spinal cord
SCG10 (red)
G
***
Axon profile length (μm)
1000
500
0
Scr 190-208 (E7P7)
190-208

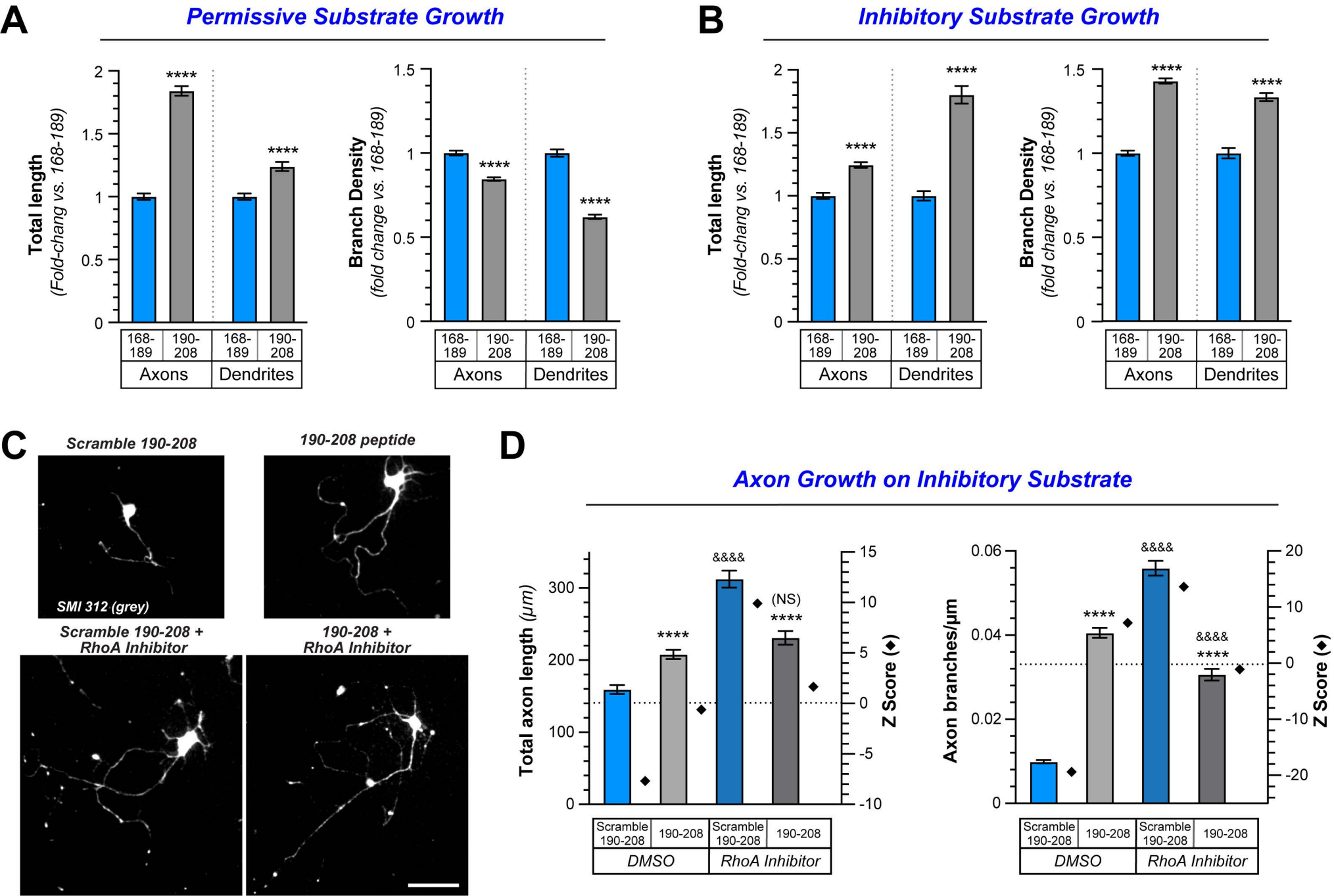
A
Permissive Substrate Growth
Total length
(Fold-chang vs. 168-189)
Branch Density
(fold change vs. 168-189)
168-189
190-208
Axons
Dendrites
B
Inhibitory Substrate Growth
C
Scramble 190-208
190-208 peptide
SMI 312 (grey)
Scramble 190-208 + RhoA Inhibitor
190-208 + RhoA Inhibitor
D
Axon Growth on Inhibitory Substrate
Total axon length (μm)
Axon branches/μm
Z Score (◆)
(NS)
Scramble 190-208
190-208
DMSO
RhoA Inhibitor

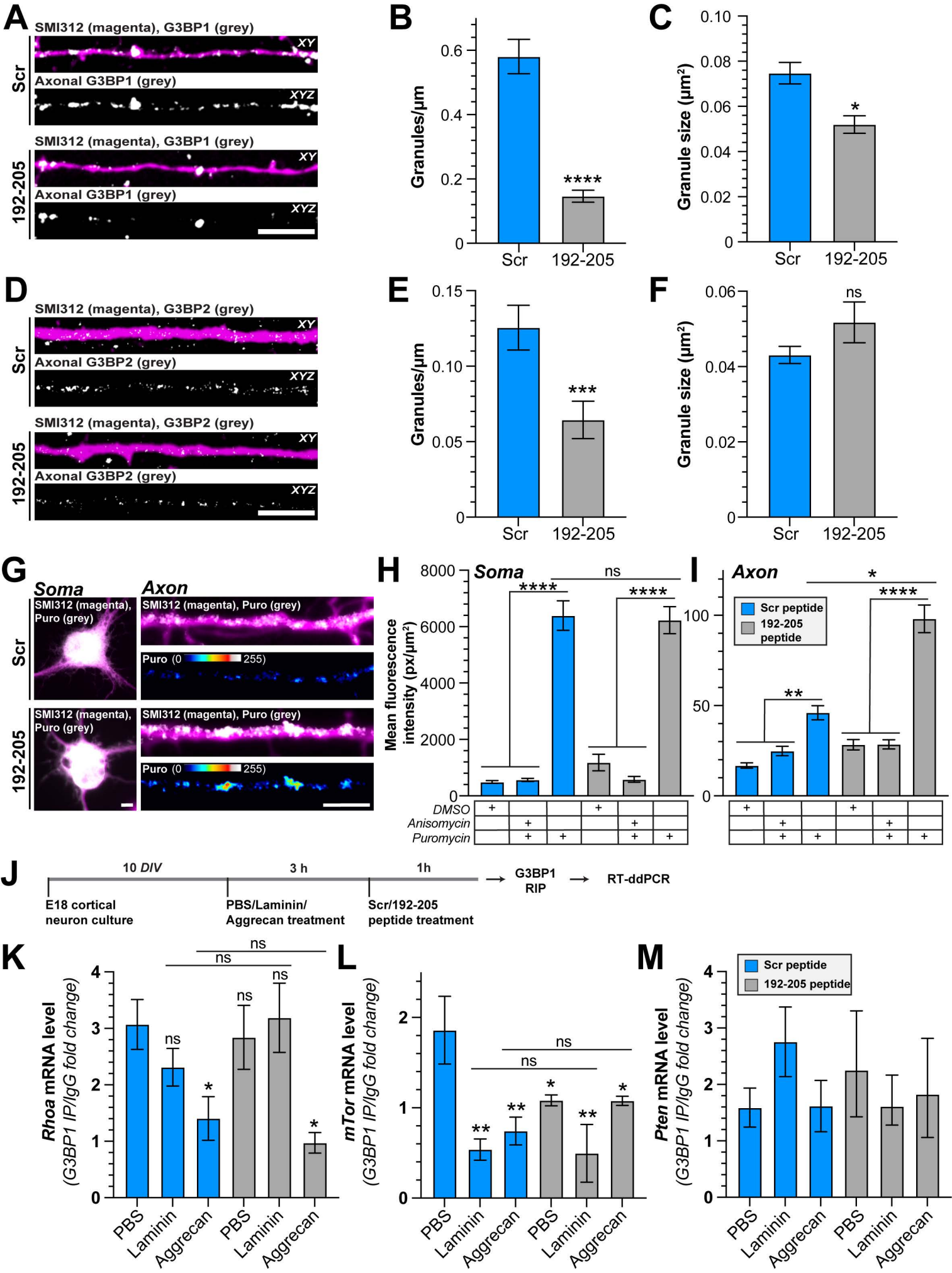
A
SMI312 (magenta), G3BP1 (grey)
XY
Axonal G3BP1 (grey)
XYZ
Scr
192-205
B
Granules/µm
****
Scr
192-205
C
Granule size (µm²)
*
D
SMI312 (magenta), G3BP2 (grey)
Axonal G3BP2 (grey)
E
***
F
ns
G
Soma
Axon
SMI312 (magenta), Puro (grey)
Puro (0 255)
H
Mean fluorescence intensity (px/µm²)
DMSO
Anisomycin
Puromycin
I
Scr peptide
192-205 peptide
J
10 DIV
3 h
1h
E18 cortical neuron culture
PBS/Laminin/ Aggrecan treatment
Scr/192-205 peptide treatment
G3BP1 RIP
RT-ddPCR
K
Rhoa mRNA level (G3BP1 IP/IgG fold change)
PBS
Laminin
Aggrecan
L
mTor mRNA level (G3BP1 IP/IgG fold change)
M
Pten mRNA level (G3BP1 IP/IgG fold change)